Science Advances

AAAS

advances.sciencemag.org/cgi/content/full/3/11/e1701450/DC1

Supplementary Materials for

Radiocarbon chronology of Manot Cave, Israel and Upper Paleolithic dispersals

Bridget Alex, Omry Barzilai, Israel Hershkovitz, Ofer Marder, Francesco Berna, Valentina Caracuta, Talia Abulafia, Lauren Davis, Mae Goder-Goldberger, Ron Lavi, Eugenia Mintz, Lior Regev, Daniella Bar-Yosef Mayer, José-Miguel Tejero, Reuven Yeshurun, Avner Ayalon, Mira Bar-Matthews, Gal Yasur, Amos Frumkin, Bruce Latimer, Mark G. Hans, Elisabetta Boaretto

Published 15 November 2017, *Sci. Adv.* **3**, e1701450 (2017)
DOI: 10.1126/sciadv.1701450

The PDF file includes:

- fig. S10. Calibrated radiocarbon dates from area E plotted by absolute elevation.
- fig. S11. Calibrated radiocarbon dates from area C plotted by absolute elevation.
- fig. S12. Bayesian models and outlier analysis.
- table S1. Lithic assemblage in area E.
- table S2. Lithic assemblage in area C.
- table S3. Radiocarbon measurements of Manot charcoal samples prepared by different pretreatments.
- table S4. Comparison of ABA and ABOx charcoal dates from Levantine EUP sites.
- table S5. Radiocarbon samples and dates for Manot Cave.
- table S6. Excavation contexts with archeological classifications and date ranges.
- table S7. Outputs of Bayesian model 1 based on cultural phases.
- table S8. Cultural phase estimates for eight runs of model 1.
- table S9. Outputs of Bayesian model 2 based on lithostratigraphic units.
- data set S1. Published dates used to construct regional chronology.
- References (*62–116*)

Other Supplementary Material for this manuscript includes the following:
(available at advances.sciencemag.org/cgi/content/full/3/11/e1701450/DC1)

data set S1 (Microsoft Excel format). Published dates used to construct regional chronology.

text S1. Levantine EUP

The Early Ahmarian and Levantine Aurignacian were two distinct archaeological industries (*4*, *5*), thought to have coexisted in the Levant for some time during the Early Upper Paleolithic (EUP) (*24*, *62*). In Early Ahmarian assemblages prismatic core reduction was used to produce elongated blanks with a soft hammer (*63*, *64*). The toolkit features retouched and backed blades, bladelets, endscrapers, burins, and el-Wad points. Bone tools and shell ornaments have been found in coastal cave sites conducive to organic preservation (*3*, *17*, *65*). The industry has been documented throughout the Levant, in caves of the Mediterranean woodlands and open-air sites of the arid regions. There is variability between assemblages classified as Early Ahmarian, which may correspond to different ecological zones or chronological changes (*19*, *25*).

The Early Ahmarian is best documented at Ksâr ʻAkil XX-XVI (*66*, *67*), Üçağızlı B3-B (*17*), Kebara IV-III (*68*), Boker A (*69*), Nahal Nizzana XIII (*70*), Abu Noshra I-II (*71*), Qadesh Barnea 9 and 601 (*72*), Lagama VII (*73*, *74*), and Tor Sadaf EUP (*75*). The easternmost Early Ahmarian assemblage was found in Syria at Wadi Kharar 16R (*25*). A juvenile skull and postcranial remains ("Egbert") were recovered from Early Ahmarian Layer XVII at Ksâr ʻAkil, and identified as modern human based on casts (*76*). Early Ahmarian layers at Üçağızlı have produced isolated teeth with ambiguous taxonomic affinities (*17*). Despite the weak fossil evidence, the Early Ahmarian is widely thought to have been developed locally from Initial Upper Paleolithic (IUP) traditions by modern humans (*26*, *64*). The Ahmarian has also been linked to the Protoaurignacian in Europe, as both contain shell ornaments and long, straight blade/lets—the latter possibly being used to arm projectile weapons (*50*). It has been argued that the Ahmarian led to the development of the Protoaurignacian through the spread of people or ideas (*1*, *6*).

Strictly defined, the Levantine Aurignacian is characterized by different reduction sequences, including production of thick blanks (blades and flakes) with hard hammer percussion and bladelet production from carinated cores/burins (*7*, *64*, *77*). Typologically, the assemblages are dominated by thick endscrapers (nosed, shouldered, carinated varieties) and also include burins, Aurignacian retouched blades, el-Wad points, and Dufour bladelets. There are personal ornaments, portable art, and osseous tools (*24*, *42*).

The best-described Levantine Aurignacian assemblages are from Ksâr ʻAkil VIII-VII (*40*), Kebara II-I (*36*, *68*, *78*), Hayonim D (*42*), Sefunim V (*79*), and Manot (*47*). The Levantine Aurignacian *sensu stricto* was stratigraphically and geographically limited, appearing intrusive within the local UP sequence to which the Ahmarian seems to have belonged (*40*). Based on this observation and the industry's typo-technological similarities with Aurignacian assemblages of Europe, some have argued that European modern humans spread Aurignacian traditions to the Levant (*7*, *24*, *37*). However, it is also unclear which particular phase of the European sequence could be the potential precursor of the Levantine Aurignacian. The Early Aurignacian of Western Europe appears similar, based on Aurignacian retouched blades, Aurignacian scrapers with scalar lateral retouch, and flat carinated items (*7*, *39*). Split-based antler points, characteristic of the Early Aurignacian, are rare in Levantine Aurignacian assemblages (*47*). On the other hand, the Evolved Aurignacian resembles the Levantine industry considering nosed and shouldered pieces, twisted Dufour bladelets, and simple-based antler points (*44*, *46*, *47*).

Furthermore, it should be stressed that some tool types used to link Levantine and European Aurignacian assemblages are found throughout the Levantine UP sequence. Dufour bladelets are found in Late UP and Epipaleolithic layers, and also appear in Ahmarian layers as the product of narrow-fronted cores and laterally carinated items (*7*, *39*). "Aurignacian" elements such as

carinated scrapers and scalar retouched blades appear in small numbers within Ahmarian assemblages (*73*, *80*). Flat carinated items, typical of the European Aurignacian, are rare in Levantine Aurignacian assemblages, while lateral carinated items are found in all Levantine Late UP industries (*81*, *82*).

Given these questions and caveats, it is difficult at this stage of research to interpret apparent similarities and infer relations between the European and Levantine Aurignacian. It is possible that the Levantine Aurignacian resulted from a number of processes, including assimilation with makers of the Ahmarian, long distance diffusion of ideas from Europe, and/or movement of hunter-gatherers from Europe to the Levant during different phases of the European Aurignacian.

text S2. Site description and archeological sequence

Located ~220 m asl in a hilly woodland, Manot Cave is in the western Galilee region of Israel, about 10 km north of Hayonim Cave and 40 km northeast of the Mt. Carmel caves (*10*, *11*, *83*–*85*). The cave comprises an elongated main hall (80 m long, 10-25 m wide, 20 m deep) and two lower chambers connected north to south (fig. S1). The original cave entrance was likely blocked by roof collapse around 30,000 years ago. Twelve excavation areas (A-L) have been opened and excavations are ongoing. Most work has concentrated on the stratified sequences in Areas C and E. The lithic assemblages from Areas E and C have been studied by L.D. and T.A., respectively. The osseous industry was studied by J.-M.T. and R.Y. (*47*, *86*) and the shell assemblage by D.B.-Y.M.

Area E is at the top of the talus slope near the modern and presumed ancient cave entrances. The area contains occupational deposits and localized surfaces that likely eroded into a steep slope covered by relatively recent colluvium (fig. S2). When excavated, the occupational deposits have emerged as partially eroded terraces, defined as archaeological horizons based on the recognition of compact semi-brecciated sediment, combustion features, and concentrations of artifacts. Between the archaeological horizons the sediment is looser and artifact-poor. The lithic assemblage in Area E totals 8,051 artifacts, presented by layer in table S1.

At the top of Area E, Unit 1 is archaeologically sterile colluvium: loose, damp soil with many rocks. Unit 2 comprises nine archaeological layers (I-IX) over ~2.5 meters. The upper Unit 2 Layers I-III have low artifact density, but contain a series of well-preserved combustion features. For instance, Locus 500 in Unit 2 Layer I (fig. S2) is a 0.6 m diameter hearth with white, calcified wood ash surrounded by a layer of burnt heated clay. Burnt flints, charcoal pieces, and bone fragments excavated from a ~0.1 m thick layer adjacent to the hearth indicate a living surface. Flint tools from Unit 2 Layers I-III (n=137) include endscrapers, various types of burins (including one on a Clactonian notch), Dufour bladelets, and partially retouched twisted bladelets. The assemblage appears to be a post-Levantine Aurignacian industry, similar to those found at Meged Rockshelter Unit 3 (*87*), Nahal Ein-Gev I (*88*), and Ksâr ʻAkil VI Phase 6 (*89*).

The lower Unit 2 Layers IV-IX contain a greater number of artifacts and numerous combustion features, which appear as oval patches of white calcified ash containing burnt bones, flints, and charcoals, surrounded and underlain by reddish then blackish sediment. The flint tools from Unit 2 Layers IV-IX (n=337) are characteristic of the Levantine Aurignacian industry with endscrapers (carinated, nosed, and flat), Aurignacian blades, and carinated burins. A few Dufour bladelets and el-Wad points were also found within the layers. The osseous tool assemblage consists of awls on bones and projectile points on antlers (*47*). A perforated red deer (*Cervus elaphus*) canine came from Unit 2 Layer V. Red deer canines were among the most frequently used personal ornaments in the European Aurignacian (*90*, *91*). The material culture from Unit 2 Layers IV-IX is similar to Hayonim Unit D (*42*), Kebara I-II (*78*), Raqefet III (*92*), Sefunim V (*79*), and probably to Ksâr ʻAkil VII-VIII Phase 5 (*40*).

The few marine shell beads (<10) in Area E are *Columbella rustica*, *Nassarius gibbosulus*, and *Antalis* sp. Large local land snails, *Levantina caesareana*, may have been consumed.

A different depositional history led to the formation of Area C near the base of the talus slope (fig. S3). The area was divided into 8 units based on changes in abundance and character of geologic and anthropogenic materials. The sediment consists of dark brown to reddish brown clay

to silty clay loam with varying compactness and density of stones. Several channels were observed that follow the natural slope of the talus. No occupational surfaces were identified. The lithic assemblage, totaling 20,748 artifacts, is presented in table S2 by unit. The units that have been dated are also the ones with larger sample sizes (2,072 in Unit 4; 9,186 in Unit 5; 4,318 in Unit 6; 3,624 in Unit 7). The debitage and debris in these units compose about 95% of the assemblage.

From the top to bottom of the excavated sequence, the tool composition shows a shift from Aurignacian to Ahmarian traditions. The flint tools in Unit 4 are characterized by Aurignacian components including carinated and nosed end-scrapers, flat end-scrapers, carinated burins, and Dufour bladelets. The osseous tools include antler projectile points (*47*) (fig. S4a:1-4). The upper portion of Unit 5 contains Aurignacian characteristics, resembling the tools in Unit 4. The lower portion of Unit 5 contains components corresponding to Aurignacian and Ahmarian traditions. The upper portion of Unit 6 is also mixed, but the bottom part of this unit shows Ahmarian components similar to those from Unit 7. The more homogenous Unit 7 best represents the Ahmarian phase at Manot Cave. It contains narrow blade cores with one or two opposing striking platforms (fig. S4b:1-2). The tools show a clear preference for blade/lets production and include el-Wad points and its variants (fig. S4b:3-8). Similar assemblages have been found in Kebara III-IV (*68*), Qafzeh E (*93*), Ksâr ʻAkil XVI-XX Phase 2 (*67*), and Üçagizli B1-3 (*17*). IUP and MP components were also recovered from the base of the excavated units of Area C (*11*).

The shell assemblage from Area C includes *Columbella rustica*, *Nassarius gibbosulus*, and a few other gastropods used for personal ornamentation as well as *Pattela* sp., probably consumed as food (*83*).

text S3. Geoarcheological results

In Area E, mineralogical analysis focused on characterization of the combustion features from which charcoals were collected for radiocarbon dating (Loci 500, 501, 502). The results of the experimental heating of control sediment show that sediment heating can be detected above 500°C, at which point the infrared OH stretching absorption band of the kaolinite lattice (3695 cm^{-1}) disappears (fig. S5). At 800°C the shoulder corresponding to the infrared OH stretching absorptions of the mica-smectite lattice (3620 cm^{-1}) disappears. Also, the major infrared Si-O silicate absorption (usually 1035 cm^{-1}) shifts to increasingly higher wavenumbers (>1070 cm^{-1}) due to increased concentration of amorphous silica derived by the dehydroxylation and melting of the clay minerals.

Because the sediment used in this experiment was from the cave base (Area A), it was particularly enriched in clay fraction and clay minerals. This sediment was chosen because it was archaeologically sterile and we were interested in transformations of the clay minerals contained in the cave sediment. Although sediment from other areas of the cave contains larger amounts of sand and silt than the control sediment, the heating experiments indicate that the clay minerals composing the substratum and sediment fragments of the combustion features were locally transformed by temperatures ranging approximately 500-800°C.

The combustion features also all contain wood ash, which was identified through microscopy as well-preserved oxalate pseudomorphs (fig. S2) and through FTIR as calcite with atomic disorder consistent with that of wood ash (*94*). Based on micromorphology, Locus 500 is a moderately well preserved *in situ* combustion feature, while Locus 501 seems to be a combustion feature that cracked and shifted slightly. It is clear that the features result from human-made fires on occupational surfaces of Area E, which were probably used at the same time as associated artifacts.

In Area C the sediment contains clay (kaolinite and illite/smectite), quartz, and carbonate-hydroxylapatite minerals (the primary component of bones, coprolites, and authigenic minerals). The same general fabric was observed throughout the section (fig. S3). The sediments have a subangular blocky microstructure with crumb microstructure in mm-cm scale passage features and burrows. The dominant mineral inclusions are sand and silt sized quartz and mica, in addition to gravel-sized brecciated soil aggregates, phosphatic nodules, phosphatized limestone fragments, coprolites, and abundant anthropogenic material (bones, flints, and charcoals). There is considerable clay translocation, levigation (b-fabric), and calcification (micritic calcite coatings, hypocoatings, impregnation, and infillings). The large quantity of apatitic coprolite fragments indicates an intense local use of the cave by carnivores (mainly hyena). *In situ* formation of aluminum or iron phosphates was not detected, indicating that Area C did not witness extensive guano accumulation. Some phosphatized sediment and coprolites formed upslope and relocated downslope to Area C. There is no evidence of anthropogenic occupational surfaces, but sedimentary surfaces are indicated by several features. These include flowstones, localized cm-thick silty clay crusts that were likely puddles, and a thin (~1 cm) layer of calcite-rich sediment overlying Unit 7, which has been interpreted as a depositional unconformity. Area C was likely formed by colluvial deposition and periodic surface stability.

text S4. Charcoal pretreatment: ABA, ABOx, and stepped combustion comparisons

The chronology of Manot is based on dates of charcoals prepared by the ABA pretreatment. In order to determine this method, four samples were separately homogenized and prepared with different pretreatments: 1) ABA, 2) ABOx, 3) ABA-SC to 630°C, 4) ABA-SC to 900 °C, 5) ABOx-SC to 630°C, and 6) ABOx-SC to 900°C. Some samples were prepared as duplicates for a given pretreatment, resulting in a total of 31 measurements in the experiment. The same background correction (0.263 ± 0.032 pMC), reflecting only graphitization and AMS steps, was applied to all fractions. Therefore differences between pMC values of the same charcoals subjected to different pretreatments indicate differences in the effectiveness of the respective pretreatments. The ABA treatment without stepped combustion consistently produced pMC values that were the smallest or among the smallest for each charcoal (table S3, fig. S6). One measurement of the ABA pretreatment provided a notably higher pMC value, although its ABA duplicate still provided the smallest pMC value for that charcoal (RTD-7816). No clear explanation has been found for this outlier.

The overall pattern of smaller pMC values and older dates from ABA treatment may be explained by the following: ABOx and stepped combustion destroy more of the original charcoal compared to ABA. Thus, any surviving clay in the ABOx and stepped combustion fractions would comprise a greater proportion of the measured sample. In the case of Manot, residual clay would result in younger dates because the total organic carbon (TOC) in sediments is younger than associated charcoals. As fig. S6 shows, the discrepancy between ABA and other treatments increases with age. This supports the interpretation that clay associated organic material is responsible for the seemingly younger ages, as the older samples have less original ^{14}C. FTIR analyses of the ABA and ABOx treated samples also supports this interpretation (fig. S7). Spectra of the ABOx treated samples have higher absorption peaks reflecting the presence of quartz and clay.

We therefore conclude that for Manot Cave charcoal samples, the ABA procedure is most appropriate. This result is consistent with the general pattern that as charcoal preservation decreases, which usually occurs with increasing age, the less harsh ABA procedure should be more appropriate. The same results and conclusion were drawn for Kebara Cave (*8*).

Previous studies have compared charcoal pretreatment procedures and obtained variable results. For numerous European Paleolithic sites, ABOx or ABOx-SC produced presumably more reliable dates (older and/or more consistent with stratigraphic information) (*13*, *14*, *95*). However, that pattern has not held for Levantine EUP sites reviewed in this paper (fig. S8, table S4). In two separate studies, charcoals from Kebara were divided and prepared by ABA and ABOx-SC, then subjected to the same graphitization and AMS procedures (*8*, *15*). In both cases, the ABA-treated fractions had older or statistically indistinguishable dates compared to their ABOx-SC-treated pairs. Moreover, in the Rebollo study, the ABA fractions had better preservation parameters and 7 ABOx-SC fractions produced %C values below 50% (*8*). For Ksâr ‘Akil and Mughr el-Hamamah, fractions of the same charcoals were dated by ABA and ABOx-SC at different times (Ksâr ‘Akil) and in different laboratories (Mughr el-Hamamah) (*9*, *19*). In these studies the ABA fractions also produced older or statistically indistinguishable radiocarbon dates. However, other steps of the procedure (vacuum lines, graphitization, AMS) may have influenced the measured 14C values. For Üçağızlı no charcoals were divided and prepared by both methods, but charcoals from Layer I produced an overlapping spread of dates whether prepared by ABA (n=4) or ABOx (n=3) (*17*).

Only the Kebara and Manot charcoals were subjected to a controlled intercomparison study. However, we also mention the results from Ksâr ‘Akil, Mughr el-Hamamah, and Üçağızlı to make the points that ABA does not *always* produce older dates, and independent parameters are needed to evaluate the reliability of dates. The samples discussed above were prepared in five different laboratories (Oxford, University of Arizona, Rafter, Aeon, and Weizmann). Within the general procedures, there is significant variation of protocols, including the monitoring of charcoal preservation parameters, the use and temperatures of stepped combustion, the strength and duration of acid/base treatments, and work in ultraclean vacuum lines (*8*, *28*, *52*, *96*, *97*). A simple comparison between ABA and ABOx dates oversimplifies the variation between laboratory protocols. The best pretreatment for charcoal most likely depends on the burial environment and preservation state of charcoals. As we have done for Manot, our approach is to tailor pretreatment to the particular charcoals and sediment, and to monitor preservation parameters (FTIR spectra, %C) throughout the protocol to qualify the sample for dating.

text S5. Charcoal preservation and radiocarbon results

The FTIR spectra of untreated samples all showed strong carboxylate (COO-) absorptions around 1575 cm^{-1} and 1385 cm^{-1}, characteristic of fossil charcoal (fig. S9) (*30, 98*). Some untreated samples also showed absorptions indicating the presence of clay, such as the silicate absorption at 1035 cm^{-1}. However these peaks were eliminated or significantly reduced in spectra after ABA treatment, suggesting that adhering sediment was effectively removed. The post-ABA spectra showed the pattern expected for pretreated fossil charcoal: carboxylic acid (COOH) absorptions at 1715 cm^{-1} and 1245 cm^{-1} as well as carboxylate absorptions at 1600 cm^{-1} and 1400 cm^{-1}.

The %C upon combustion measurements of nearly all charcoals were greater than 50% (table S5). A value less than 50% suggests that the material may not be pure charcoal (*8, 99*). Five samples did not meet this requirement, but other lines of evidence suggest that these dates are reliable: the %C values are still above 40%, the FTIR spectra indicate pure pretreated charcoal, and the dates are consistent with the samples' stratigraphic positions. We note that 3/5 of the charcoals with <50% C came from combustion features. It is possible that charcoal preservation was poorer in combustion features, in which the microenvironment may have caused greater diagenesis and formation of carboxylate groups.

The samples treated with water-base-acid (WBA), due to small sample size, produced dates consistent with dates from samples treated by the standard ABA procedure (table S5). Statistically indistinguishable radiocarbon dates were produced for fractions of the one charcoal treated by both methods (RTD-7088). The WBA-fraction had higher % efficiency and %C values. Samples divided and graphitized on the ultraclean and standard lines produced consistent results. The exception was sample RTD-7784, which had a significantly older radiocarbon date for the ultraclean line fraction (RTD-7784.1).

Radiocarbon measurements were also produced on the total organic carbon (TOC) of sediment samples removed from 4 dated charcoals from Area C. The TOC reflects any organic carbon in the sediment, which is a mixture of clay, degraded organic matter, and recent organic growth. Inorganic carbon from carbonate minerals and bones was removed by acid dissolution. The sediment TOC dates range from 35-29 ka cal BP, or 16,000-10,000 years younger than the associated charcoals. Therefore if any sediment survived the pretreatment procedure, we would expect this contamination to make the charcoal radiocarbon dates younger than their true ages. However the TOC was very low, constituting only ~0.8% of the insoluble fraction of clay.

All dates from Manot were calibrated with OxCal v4.2 (*59*) and the IntCal13 curve (*60*) (Figs. 2-3, table S5, figs. S10-S11). The archaeological chronology is based on charcoals from combustion features of Area E and the J squares in Area C (Table 1, table S6). In Area E, charcoals (n=6) producing dates of 34-33 ka cal BP were collected from two combustion features (*Loci 500, 501*) in Unit 2 Layer I, classified as post-Levantine Aurignacian. Two charcoals produced dates 37-36 ka cal BP and came from a combustion feature (*Locus 502*) in Unit 2 Layer IV, classified as Levantine Aurignacian. An additional charcoal from the Unit 1 colluvium produced a date of 35-34 ka cal BP.

In Area C a nearly continuous ~1.5 meter sequence of radiocarbon dates was produced from 23 charcoals from Squares J64, J65, and J66 (fig. S11). Unit 4, which contained predominately Aurignacian artifacts, had charcoal dates (n=7) from 38-34 ka cal BP. Units 5-6 contained a mixture of Ahmarian and Aurignacian artifacts. Charcoals from these units (n=14) clustered into a

younger set of 38-34 ka cal BP higher in the section and an older set of >42 ka cal BP lower in the section. Charcoals (n=2) from Unit 7, classified as Ahmarian, produced dates of 46-44 ka cal BP. There is no clear stratigraphic boundary between Ahmarian and Aurignacian materials in Area C. However, it is our assumption that the younger charcoals from the upper portion of Unit 5 (above z=205.50) represent Aurignacian occupations because they overlap in age with dates from other Aurignacian contexts: the overlying Unit 4 as well as the *in situ* combustion feature in Area E Unit 2-IV. Likewise, we assume that the older charcoals from the lower portion of Unit 5 (below 205.35), which overlap in age with dates from Ahmarian Unit 7, represent Ahmarian occupations.

At the boundary of Units 5/6, between the dates that we attribute to Aurignacian and Ahmarian phases, are three samples (RTD-7783A, RTD-7785, RTD-7786) that do not show age-depth consistency. The charcoals came from a 15 cm portion of the section (z=205.50 to 205.35) that is characterized by many rocks, suggesting water disturbance. There also appears to be a gap in dates from 41-39 ka cal BP. The interstratified dates and temporal hiatus likely reflect the complicated depositional history of this portion of the sequence. We did not include these dates in the cultural chronology.

Additional dates were produced from two other contexts to answer questions about site formation processes. Charcoals (n=5) and sediment (n=2) were measured from Area C Square I65 (between the J square sequence and cave wall) in order to assess the degree of mixing and potential noise in the sequence. The artifacts in I65, while representative of Ahmarian and Aurignacian, reflect size sorting due to greater water activity near the cave wall. The charcoals dated to 39-31 ka cal BP. This is a wider range, but overlaps with dates from the equivalent elevation in J65 (table S5, fig. S11). The dates support the assumption that mixing is more significant in the I squares and that the J squares have a better-preserved archaeological sequence. However, the degree of mixing in I65 is still surprisingly low for a Pleistocene deposit at the bottom of a talus next to the cave wall.

In order to compare the age results of U-Th and radiocarbon dates, several charcoals (n=4) were dated from between flowstone layers in Area C Square M65 (*11*). The area represents a channel and was not assigned to a lithostratigraphic unit, although artifacts were recovered. Speleothem samples were collected from 4 flowstone layers. The uppermost lamina of the top flowstone (sample 1023) produced a U-Th date of 20 ± 0.3 ka, while the lowermost flowstone (sample 1028) produced a U-Th date of 42.0 ± 1.8 ka. Charcoal samples were collected from between the base of the top flowstone (sample 1024: U-Th date of 32.4 ± 1.1 ka) and the next lowest flowstone (sample 1054: U-Th date of 32.1 ± 0.5 ka). The radiocarbon dates ranged from 31-27 ka cal BP. Thus the U-Th and radiocarbon results are in good agreement.

text S6. Bayesian modeling

We constructed several Bayesian models in order to test how different assumptions about the depositional history of Manot Cave affect the posterior dates and spans of archaeological phases (fig. S12). However, we report the unmodeled ranges for conclusions in the main text because these ranges are not influenced by our assumptions, defined as model parameters. The models below constrain the likelihood of dates by stratigraphic priors, estimate phase spans, and formally test for outliers (*59, 100*). All dates were set with the standard 5% prior likelihood of being an outlier in a t-type outlier model. The OxCal Date command was used to estimate the spans of phases.

Model 1, the cultural span model, is based on the following reconstruction of the depositional history: a package of Ahmarian material was redeposited in Area C from primary contexts upslope. An unspecified amount of time later, the Ahmarian package was overlain by a package of Aurignacian material through the same process of secondary deposition from primary contexts upslope. In Area E *in situ* Aurignacian materials were overlain by *in situ* materials from the post-Levantine Aurignacian industry.

Based on these assumptions, Model 1 constrains dates to three sequential phases of Ahmarian > Aurignacian > post-Levantine Aurignacian (table S7). Within a given phase, the dates are not ordered because it is likely that materials within phases of Area C (the Ahmarian and Aurignacian packages) were mixed when they were redeposited. Moreover, this model parameter avoids placing an order between Aurignacian materials from Areas C and E, which is unknown. Aurignacian-associated dates from Areas C and E belonged to the same phase and are not ordered. The boundaries between phases are sequential, so that a given phase occurs some unspecified amount of time before its succeeding phase. The alternative of contiguous boundaries would force each phase to end immediately before its succeeding phase. While this is possible at Manot, it is not evident from stratigraphy. Sequential boundaries provide a more conservative constraint on the dates.

The Ahmarian phase includes dates from Area C Unit 7 and the lower portion of Area C Unit 6 (below z=205.35). The Aurignacian phase includes dates from Area E Unit 2 Layer IV (combustion feature Locus 502), Area C Unit 4, and the upper portion of Area C Unit 5 (above z=205.50). The post-Levantine Aurignacian phase includes dates from Area E Unit 2 Layer I (combustion features Loci 500 and 501).

There was no clear stratigraphic or artifact based boundary between the Ahmarian and Aurignacian phases in Area C. However it is our working assumption that the younger dates from the top of Unit 5 that overlap in age with dates from other Aurignacian contexts belong to the Aurignacian phase. Likewise, we assume that the older dates from the bottom of Unit 6 that overlap in age with dates from the underlying Ahmarian Unit 7 belong to the Ahmarian phase. Stratigraphically between these included dates is the boundary between Units 5/6 and three dates that show reverse stratigraphy (RTD-7783A, RTD-7785, RTD-7786). This portion of the sequence appeared to be more mixed due to water activity and therefore these dates were omitted from the model. Usually dates should not be eliminated “by hand” when using outlier analysis (*101*). However, we consider this portion of the sequence to be disturbed and not reflective of the chronology of human occupations. Moreover, these dates *were* included and identified as outliers in Model 2 (below), which placed dates in Area C into sequences based on lithostratigraphic unit.

Model 1 Oxcal code:

```
Plot()
 {
  Outlier_Model("General",T(5),U(0,4),"t");
  Sequence()
  {
   Boundary("Start Ahmarian");
   Phase("Ahmarian")
   {
    R_Date("RTD7196", 41100, 454)
    {
     Outlier("General", 0.05);
    };
    R_Date("RTD7115", 42210, 385)
    {
     Outlier("General", 0.05);
    };
    R_Combine("RTD7197-combine")
    {
     R_Date("RTD7197.1", 37332, 300);
     R_Date("RTD7197.2", 37118, 299);
     Outlier("General", 0.05);
    };
    R_Date("RTD7117", 41610, 540)
    {
     Outlier("General", 0.05);
    };
    R_Date("RTD7119", 42310, 375)
    {
     Outlier("General", 0.05);
    };
    R_Date("RTD7118", 40280, 320)
    {
     Outlier("General", 0.05);
    };
    R_Date("RTD7116", 48705, 700)
    {
     Outlier("General", 0.05);
    };
    R_Date("RTD7087", 41790, 380)
    {
     Outlier("General", 0.05);
    };
    R_Date("RTD7086", 38875, 305)
    {
     Outlier("General", 0.05);
    };
   };
   Boundary("End Ahmarian");
   Boundary("Start Aurignacian");
   Phase("Aurignacian")
   {
    R_Combine("RTD7784-combine")
    {
     R_Date("RTD7784.1", 33743, 289);
     R_Date("RTD7784.2", 32920, 145);
     Outlier("General", 0.05);
    };
    R_Date("RTD7816", 33207, 157)
    {
```

```
 Outlier("General", 0.05);
 };
 R_Combine("RTD7194-combine")
 {
  R_Date("RTD7194.1", 32241, 191);
  R_Date("RTD7194.2", 32543, 201);
  Outlier("General", 0.05);
 };
 R_Combine("RTD7195-combine")
 {
  R_Date("RTD7195.1", 33129, 210);
  R_Date("RTD7195.2", 32382, 201);
  Outlier("General", 0.05);
 };
 R_Date("RTK6305", 32135, 500)
 {
  Outlier("General", 0.05);
 };
 R_Date("RTK6304", 32135, 500)
 {
  Outlier("General", 0.05);
 };
 R_Date("RTK6624", 33290, 505)
 {
  Outlier("General", 0.05);
 };
 R_Date("RTK6303", 31870, 500)
 {
  Outlier("General", 0.05);
 };
 R_Date("RTK6307", 32730, 530)
 {
  Outlier("General", 0.05);
 };
 R_Date("RTK6306", 30865, 420)
 {
  Outlier("General", 0.05);
 };
 R_Date("RTK6308", 30390, 400)
 {
  Outlier("General", 0.05);
 };
 Line( );
 R_Date("RTD7247", 32272, 192)
 {
  Outlier("General", 0.05);
 };
 R_Date("RTD7246", 32685, 200)
 {
  Outlier("General", 0.05);
 };
};
Boundary("End Aurignacian");
Boundary("Start post-Aurignacian");
Phase("post-Aurignacian")
{
 R_Date("RTD7089",  29720, 150)
 {
  Outlier("General", 0.05);
 };
 R_Combine("RTD7088-combine")
```

```
  {
   R_Date("RTD7088A", 29230, 200);
   R_Date("RTD7088B", 29060, 145);
   Outlier("General", 0.05);
  };
  R_Date("RTK6847.1", 29488, 383)
  {
   Outlier("General", 0.05);
  };
  R_Date("RTD7242", 29458, 154)
  {
   Outlier("General", 0.05);
  };
  R_Date("RTD7243", 29031, 147)
  {
   Outlier("General", 0.05);
  };
  R_Date("RTD7244", 29087, 150)
  {
   Outlier("General", 0.05);
  };
 };
 Boundary("End post-Aurignacian");
};
Sequence("Ahmarian")
{
 Boundary("=Start Ahmarian");
 Date("Ahmarian");
 Boundary("=End Ahmarian");
};
Sequence("Aurignacian")
{
 Boundary("=Start Aurignacian");
 Date("Aurignacian");
 Boundary("=End Aurignacian");
};
Sequence("post-Aurignacian")
{
 Boundary("=Start post-Aurignacian");
 Date("post-Aurignacian");
 Boundary("=End post-Aurignacian");
};
};
```

Model 1 produces consistent phase estimates for the post-Levantine Aurignacian industry from 33.8-33.3 ka cal BP and the Aurignacian between 37.2-35.2 ka cal BP (fig. S12, tables S7-S8). The model has low convergence for the start of the Ahmarian due to RTD-7116, a sample from midway through Unit 6 that is 48,700 ^{14}C yr BP, or ~2000 years older than any other radiocarbon date from Manot. The date extends beyond the 50 ka cal BP limit of the calibration curve at 95.4% probability and therefore may be beyond the age limit of the radiocarbon method. Outputs of Model 1 either: 1) estimate the Ahmarian from 46-42 ka cal BP and identify RTD-7116 as an outlier with >50% likelihood or 2) estimate the Ahmarian from 49-42 ka cal BP and do not identify RTD-7116 as an outlier (table S8). Sample RTD-7116 may belong to Ahmarian deposits or have intruded from an earlier phase such as the IUP or MP. In either case, it is clear that the Ahmarian began by at least 46 ka cal BP.

In Model 2, the stratigraphic sequence model, we tested the assumption that materials in Area C were deposited in sequence and preserve increasing age with depth. Dates from Area C were

constrained to a model of four contiguous sequences based on lithostratigraphic layer. Within each unit the dates were ordered.

Model 2 OxCal code:

```
Plot()
 {
  Outlier_Model("General",T(5),U(0,4),"t");
  Sequence()
  {
   Boundary("Start Unit 7");
   Sequence("Unit 7")
   {
    R_Date("RTD7196", 41100, 454)
    {
     Outlier("General", 0.05);
    };
    R_Date("RTD7115", 42210, 385)
    {
     Outlier("General", 0.05);
    };
   };
   Boundary("Transition Unit 7/Unit 6");
   Sequence("Unit 6")
   {
    R_Combine("RTD7197-combine")
    {
     R_Date("RTD7197.1", 37332, 300);
     R_Date("RTD7197.2", 37118, 299);
     Outlier("General", 0.05);
    };
    R_Date("RTD7117", 41610, 540)
    {
     Outlier("General", 0.05);
    };
    R_Date("RTD7119", 42310, 375)
    {
     Outlier("General", 0.05);
    };
    R_Date("RTD7118", 40280, 320)
    {
     Outlier("General", 0.05);
    };
    R_Date("RTD7116", 48705, 700)
    {
     Outlier("General", 0.05);
    };
    R_Date("RTD7087", 41790, 380)
    {
     Outlier("General", 0.05);
    };
    R_Date("RTD7086", 38875, 305)
    {
     Outlier("General", 0.05);
    };
    R_Combine("RTD7786-combine")
    {
     R_Date("RTD7786.1", 28936, 180);
     R_Date("RTD7786.2", 28850, 104);
     Outlier("General", 0.05);
```

```
 };
 R_Combine("RTD7785-combine")
 {
  R_Date("RTD7785.1", 32405, 260);
  R_Date("RTD7785.2", 32899, 146);
  Outlier("General", 0.05);
 };
};
Boundary("Transition Unit 6/Unit5");
Sequence("Unit 5")
{
 R_Date("RTD7783A", 36993, 434)
 {
  Outlier("General", 0.05);
 };
 R_Combine("RTD7784-combine")
 {
  R_Date("RTD7784.1", 33743, 289);
  R_Date("RTD7784.2", 32920, 145);
  Outlier("General", 0.05);
 };
 R_Date("RTD7816", 33207, 157)
 {
  Outlier("General", 0.05);
 };
 R_Combine("RTD7194-combine")
 {
  R_Date("RTD7194.1", 32241, 191);
  R_Date("RTD7194.2", 32543, 201);
  Outlier("General", 0.05);
 };
 R_Combine("RTD7195-combine")
 {
  R_Date("RTD7195.1", 33129, 210);
  R_Date("RTD7195.2", 32382, 201);
  Outlier("General", 0.05);
 };
 R_Date("RTK6305", 32135, 500)
 {
  Outlier("General", 0.05);
 };
 R_Date("RTK6304", 32135, 500)
 {
  Outlier("General", 0.05);
 };
};
Boundary("Transition Unit 5/Unit4");
Sequence("Unit 4")
{
 R_Date("RTK6624", 33290, 505)
 {
  Outlier("General", 0.05);
 };
 R_Date("RTK6307", 32730, 530)
 {
  Outlier("General", 0.05);
 };
 R_Date("RTK6303", 31870, 500)
 {
  Outlier("General", 0.05);
 };
```

```
   R_Date("RTK6306", 30865, 420)
   {
    Outlier("General", 0.05);
   };
   R_Date("RTK6308", 30390, 400)
   {
    Outlier("General", 0.05);
   };
  };
  Boundary("End Unit 4");
 };
};
```

Under the constraints of this model, 5 out of 23 dates were identified as outliers with >50% likelihood (fig. S12, table S9). The same outliers were identified by a model of one sequence of all dates, with no subdivision by lithostratigraphic unit. The outliers include dates from the Unit 5/6 boundary that we do not consider representative of the cultural sequence as well as RTD-7116, the oldest radiocarbon date from Manot. Additionally RTD-7197 and RTD-7087 were identified as outliers because they deviate from increasing age with depth. However, if the constraints are relaxed so that within a given phase dates do not need to fall in temporal order (as in Model 1), these dates are not outliers; they fall within the range of other Ahmarian dates with which they are associated.

text S7. Regional chronology

Our regional chronology was constructed from published radiocarbon dates from Üçağızlı, Ksâr ‘Akil, Kebara, and Mughr el-Hamamah in addition to the new dates from Manot Cave reported here (Fig. 3, data set S1). Included dates were produced from charcoals and shells. No bones from the sites produced sufficient collagen for radiocarbon dating. Dates reported in original publications that the authors rejected (and excluded from phase estimates or Bayesian models) because the sample failed predetermined preservation standards or came from poor contexts (e.g. burrow or subsurface layer) were included in dataset S1 in gray, but not depicted in Fig. 3. Dates that were included in authors’ Bayesian models (both dates that were accepted by the models and those identified as outliers) were included in both our dataset S1 and Figure 3. Individual dates were calibrated with Intcal13 for terrestrial samples (charcoal) and Marine13 for marine samples (shell) using Oxcal v4.2 (*59*, *60*). Some authors have applied a Mediterranean local reservoir correction to marine samples ($\Delta R=58 \pm 85$ ^{14}C years). Because it has not been demonstrated that this correction is appropriate for samples older than 6000 cal BP (*102*), we did not use it.

We also display authors’ reported phase ranges produced by Bayesian modeling (Fig. 3). The calibration and phase modeling procedures differ between studies and are reviewed in the following subsections. Some of the ranges were produced with the previous calibration curve IntCal-Marine09 (*103*) and/or the Mediterranean reservoir correction (*102*). We did not recalibrate and recalculate the phases because for some studies the models were not described in sufficient detail to reproduce. We prefer to compare the reported ranges, which are influenced by the assumptions and choices of the authors, as well as the unmodeled calibrated dates, which are less subjective.

Üçağızlı

Üçağızlı Cave in southern Turkey was first excavated by Minzoni-Deroche in the 1980s and then by a team from Ankara University and the University of Arizona in the late 1990s/early 2000s (*17*, *104*). The more recent excavations revealed a 3.5-meter sequence of *terra rossa* clay and silty clay. As the lithology of the sediments was relatively homogenous, stratigraphic units were defined by changes in the abundance and character of anthropogenic material. In the upper layers (B1-B3) artifacts were found as a massive accumulation, while in the lower layers (H, H1-3, I) anthropogenic material was in thin, discrete lenses. Layers B-C, classified as Early Ahmarian, were characterized by an abundance of narrow, regular blade blanks removed from bi-directional prismatic cores. The dominant tools were endscrapers, retouched blades, and pointed blades including el-Wad points. Layers D-E had low artifact yields but were most similar to the Early Ahmarian layers. Layers F-I were classified as IUP with high frequencies of wide, flat blades with facetted platforms, which were mostly produced from unidirectional parallel or convergent reduction with likely hard-hammer percussion. Endscrapers were the most abundant tool. Bone tools were found throughout the sequence, although relatively rare. Shell beads were abundant in all layers, becoming more diverse in type in more recent layers.

Radiocarbon dates were reported by Kuhn et al. (*17*), produced from mostly “what appeared to be carbonized plant material” as well as two marine mollusk shells, which were confirmed to be aragonite by FTIR spectroscopy (*105*). Ten charcoals were prepared by ABOx and the three samples that survived produced indistinguishable dates from those prepared by ABA. The dates generally showed increasing age with depth between 45-35 ka cal BP, but samples from the lowest layers were widely dispersed. An additional eight dates were produced from shells (*3*). Douka combined both sets of dates into a Bayesian model of ten contiguous phases based on

excavation layers. Under this constraint, the IUP ranged from 45/43-39/38.5 ka cal BP and the Early Ahmarian followed until 36.5/35.5 ka cal BP. Eleven of the 32 dates were outliers.

Our regional chronology displays calibrated dates of all charcoals and shells produced in both studies (*3*, *17*). Dates from layers D-E were assigned as "other" industry because the artifacts were too few for distinction between IUP or Early Ahmarian according to the authors. We also show the phase ranges reported by Douka (*3*) based on the modeled start and end dates (68.2%) for the IUP and Ahmarian (including layers D-E) phases using IntCal-Marine09.

Ksâr 'Akil

Much attention has focused on Ksâr 'Akil, Lebanon as its 23 meters of stratified archaeological deposits serve as the reference sequence for the Levantine UP and modern human remains were found in IUP and EUP layers (*9*). The rock shelter was excavated between 1937-1938 and 1947-1948 under Doherty, Ewing, and Murphy (*106*) as well as between 1969-1975 under Tixier (*107*). The earlier excavations did not apply modern excavation methods and Tixier's excavation did not reach EUP or earlier levels (*9*). The sequence has been divided into eight main archaeological phases: Mousterian (excavation levels XXXVII-XXVI), IUP (XXV-XXI), Early Ahmarian (XX-XVI), a possible occupational hiatus (XV-XIV), UP Phase 3 (XIII-XI), UP Phase 4 (X-IX), Levantine Aurignacian Phase 5 (VIII-VII), Atlitian UP Phase 6 (VI), and Epipaleolithic (V-I) (*9*, *40*, *66*, *67*, *89*, *108*).

The IUP levels contained blade cores with faceted platforms and converging sides that were used to produce elongated blanks likely by soft hammer percussion. The toolkit included chamfered pieces, end scrapers, and burins. In the Early Ahmarian levels parallel-sided cores with opposed platforms were used to produce thinner blade blanks, again, likely by soft hammer direct percussion. The toolkit included endscrapers, retouched blades and bladelets, and el-Wad points (*109*). The remaining UP levels have been difficult to classify, but Phase 5 layers VIII-VII are thought to be Levantine Aurignacian (*40*). Phase 5 is characterized by flake production, thick nosed and shouldered scrapers, invasive retouch, and a large number of bone/antler tools. Occurring at lesser frequency, blades and bladelets were mostly straight or curved, but sometimes twisted.

During the 1938 excavation season a human skull and postcranial remains were recovered within Early Ahmarian levels XVII or XVIII. The fossils have been lost, but based on descriptions and reconstructed casts of the skull, they are believed to represent a juvenile modern human, known as Ksâr 'Akil 1 or "Egbert" (*76*). A partial maxilla from a separate individual, Ksâr 'Akil 2 or "Ethelruda," was discovered in the 1947-1948 excavation in the level XXV, associated with the IUP industry. The specimen was originally described as "Neandertaloid" (*110*), but it has since been argued to represent a modern human (*9*).

Mellars and Tixier reported radiocarbon dates produced from charcoal and clay as well as Uranium series dates of bones (*61*). Two recent studies (*9*, *18*) dated marine shells and combined the new dates with the previously published ones in Bayesian models. Douka and colleagues (*9*) dated mostly ornamental shells, while Bosch and colleagues (*18*) dated dietary shells.

Our regional chronology presents the dates reported in these three studies (*9*, *18*, *61*), but we exclude the U-series dates and radiocarbon dates of clay, land snail, and bone prepared without ultrafiltration. Phases 3-4 and 6 contain UP industries that we classify as "other or undetermined." We present the modeled phase ranges produced by the Douka and Bosch studies from the beginning of the reported start dates to the end of the reported end dates (68.2%). In the Douka study, the end dates (their model 2) were 43.2-42.5 ka cal BP for the Mousterian, 41.6-40.9 ka cal BP for the IUP, 39-37.5 ka cal BP for the Early Ahmarian, and 35-34 ka cal BP for the Levantine Aurignacian (Phase 5) using Intcal-Marine09 with the Mediterranean reservoir correction. The

start of the IUP and MP are reported as unknown. Nine out of 39 dates were identified as outliers. In the Bosch study (their model 1), the IUP occurred between 44.6-43.2 ka cal BP and the Early Ahmarian occurred between 43.3-42.8 ka cal BP using Intcal-Marine13 with the Mediterranean reservoir correction. In this model 6/16 dates were determined to be outliers and then removed from the model. The models have been debated (*101*, *111*).

Kebara

Kebara Cave in Mt Carmel, Israel was excavated in multiple campaigns during the 20th century and most recently between 1982-1990 by Bar-Yosef and Vandermeersch (*112*). The 14 layers identified in the most recent excavations include Mousterian (XIV-V), Early Ahmarian (IV-III), and Levantine Aurignacian (II-I) assemblages. No diagnostic IUP artifacts were recovered and the missing phase may be explained by an unconformity between the final MP and first Early Ahmarian layer. A Neanderthal burial was discovered in Layer XII. The Mousterian Layers XII-VI have been dated by TL measurements of 38 burnt flints (*113*).

Radiocarbon dates have been produced for Kebara by several laboratories using different protocols (*8*, *15*, *68*). When the same charcoal pieces were subjected to ABA and ABOx-SC pretreatments, Brock & Higham (*15*) found no difference in the resulting ages, while Rebollo and colleagues produced older dates and better preservation parameters with the ABA treatment (*8*). Using ABA and ABOx-SC samples that passed preservation parameters, Rebollo et al. modeled the end of the MP at 48/49 ka cal BP and the start of the Ahmarian at 47/46 ka cal BP (68.2%).

Our regional chronology excluded Kebara dates from charred bone and charcoals that had %C upon combustion <50%. When an individual charcoal was prepared by different procedures, we combined the dates unless a replicate failed preservation parameters (%C<50) or had a substantially worse precision. Figure 3 shows the modeled end date for the MP and start date for the Ahmarian (68.2%) produced by Rebollo et al. (*8*) using IntCal09.

Mughr el-Hamamah

Mughr el-Hamamah in the Jordan Valley was excavated in 2010 by Stutz (*19*). Two test trenches inside Cave 2, totaling an area of 8 m^2, contained mixed modern/Pleistocene Layer A above Pleistocene Layer B. Ongoing lithics analysis suggests that the Layer B assemblage is EUP, but does not fit into the categories of IUP or Early Ahmarian, as defined by the Mediterranean coastal sites (*62*, *114*). The Layer B assemblage includes Early Ahmarian core reduction strategies and tools including el-Wad points, in addition to IUP technological characteristics and tool types such as Emireh points and chanfrein pieces. According to the authors, "it is yet unclear whether the assemblage is best described as a variant of the Initial Upper Paleolithic/Emiran, the Early Ahmarian, or a third Levantine EUP industry or industrial facies that combines elements of the former" (pg. 161) (*19*). Charcoals were collected from within or under ash lenses associated with hearths or from under what the authors describe as anthropogenic limestone slabs and a basalt cobble manuport. Charcoals were prepared by ABA (*115*) and ABOx-SC (*19*) in different laboratories and studies. The authors favored the ABOx-SC dates and report a single-phase occupation between 45-39 ka cal BP, using Intcal13 up to 50 ka cal BP and CalPal-Hulu 2007 for 50 – 59 ka cal BP (*116*). We included both sets of dates (ABA and ABOx-SC), but calibrated with IntCal13. We excluded the date on humics (Aeon-1038).

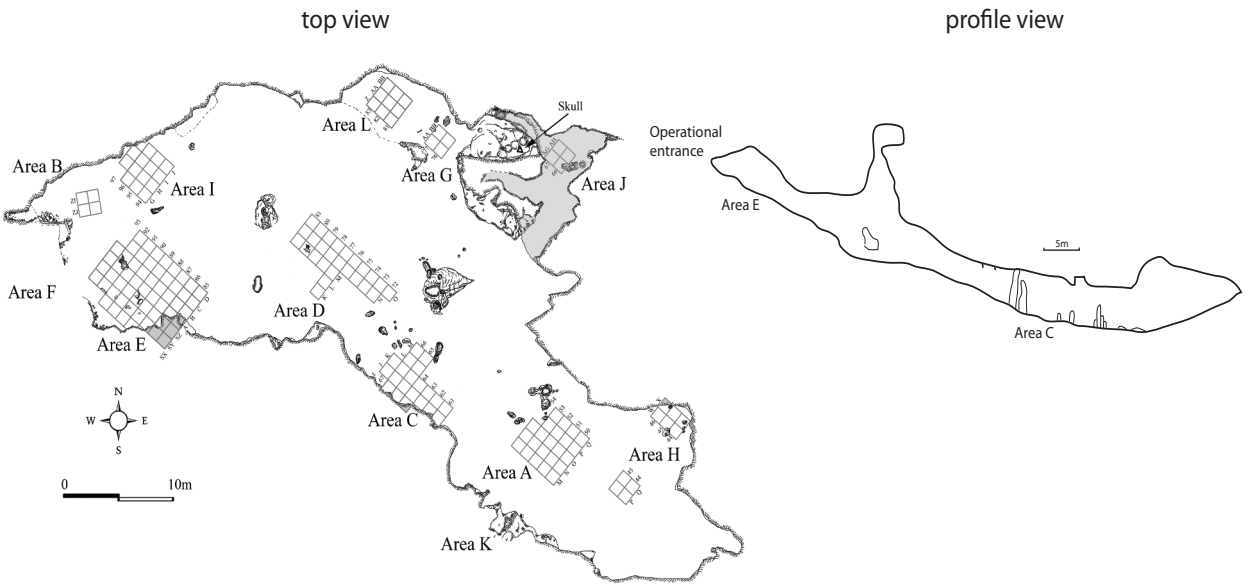

fig. S1. Top view and profile view of Manot Cave.

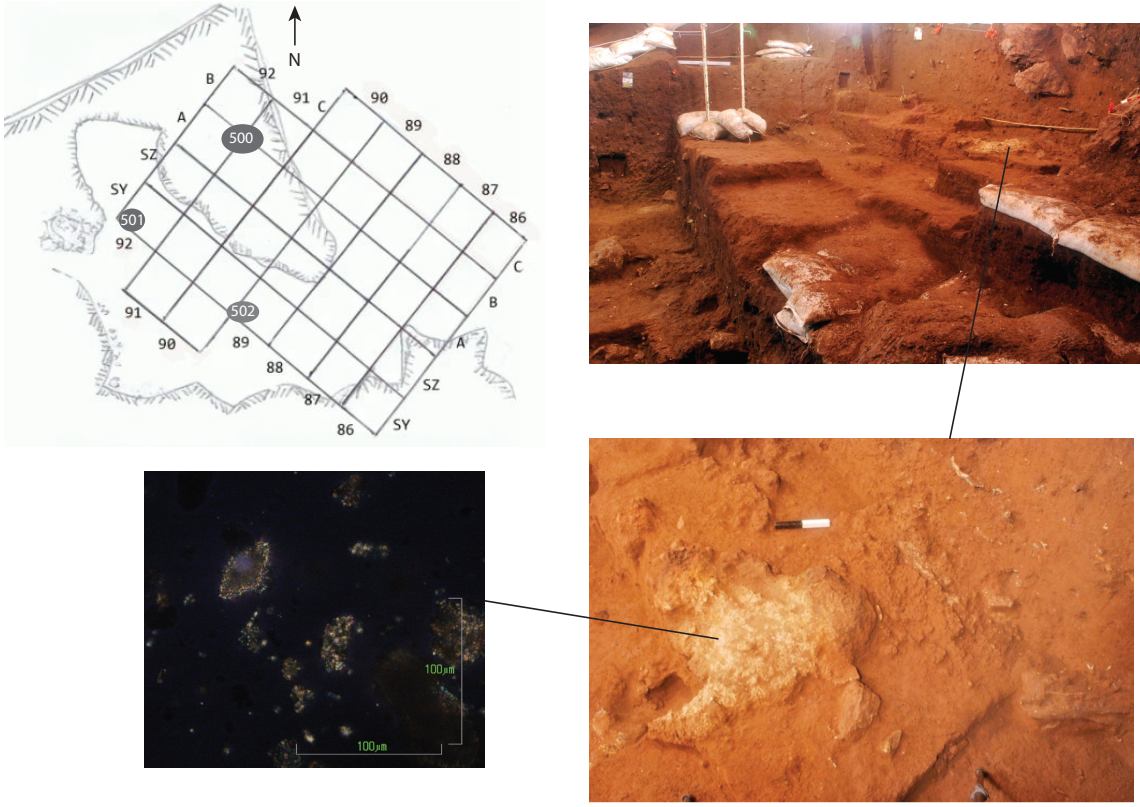

fig. S2. Excavation area E with combustion features. Clockwise from top left: (A) Top plan of Area E showing combustion features Loci 500, 501, and 502 from which charcoals were taken for radiocarbon dating. (B) View of Area E facing southwest. (C) Top view of Locus 500. (D) Image of rhombus-shaped ash pseudomorphs found in Locus 500 using a petrographic microscope with cross polarized light.

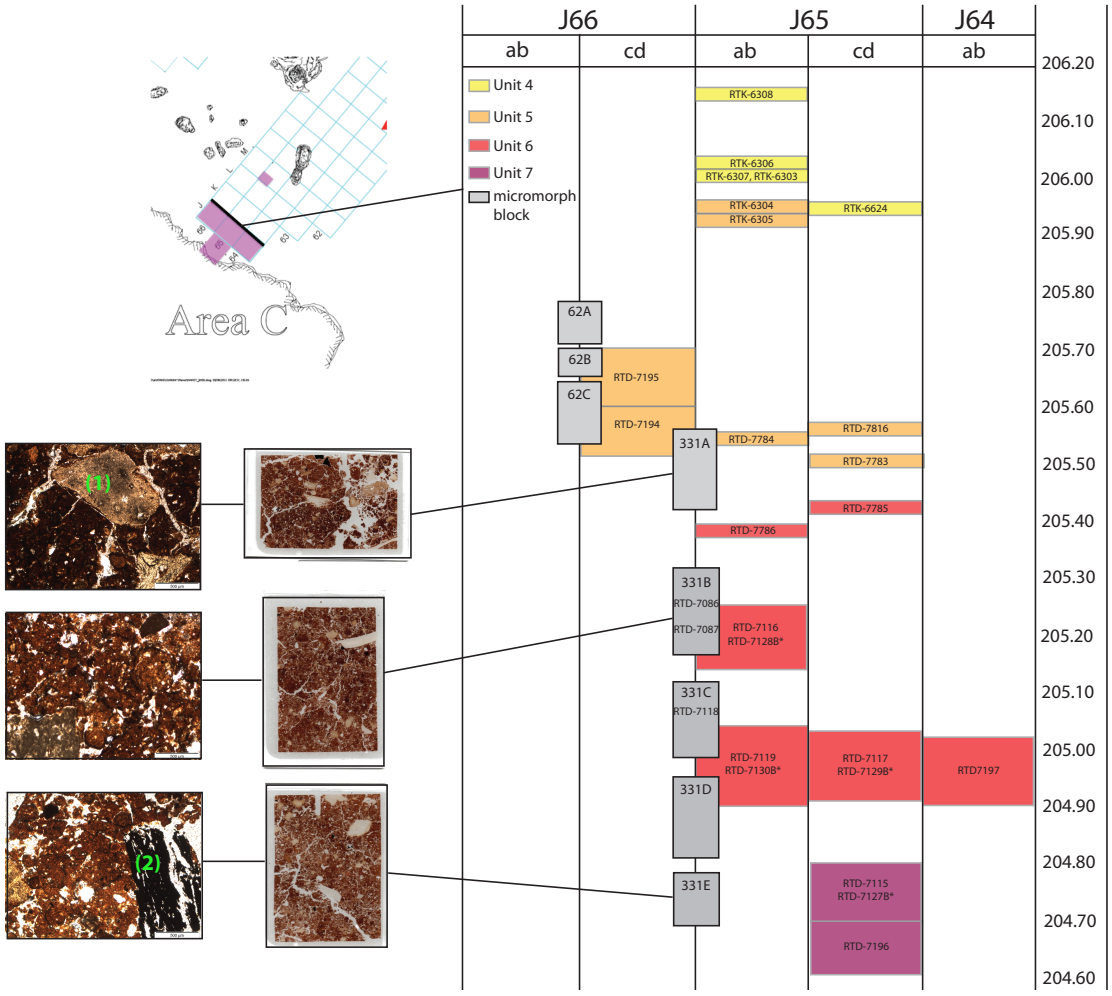

fig. S3. Area C showing locations of radiocarbon samples and micromorphology blocks. Section of Squares J66, J65, J64. The laboratory code of radiocarbon dates are listed within their excavation basket, plotted by provenience and color-coded by stratigraphic unit. Dates with * are sediment samples that were collected with associated charcoal. Micromorphology blocks are shown in gray with thin sections (75x50 mm) and micrographs under plane polarized light. The thin sections show homogeneous composition and microstructure throughout the section. The micrographs show characteristic fabric and inclusions including phosphatic nodules (1) and microcharcoal (2).

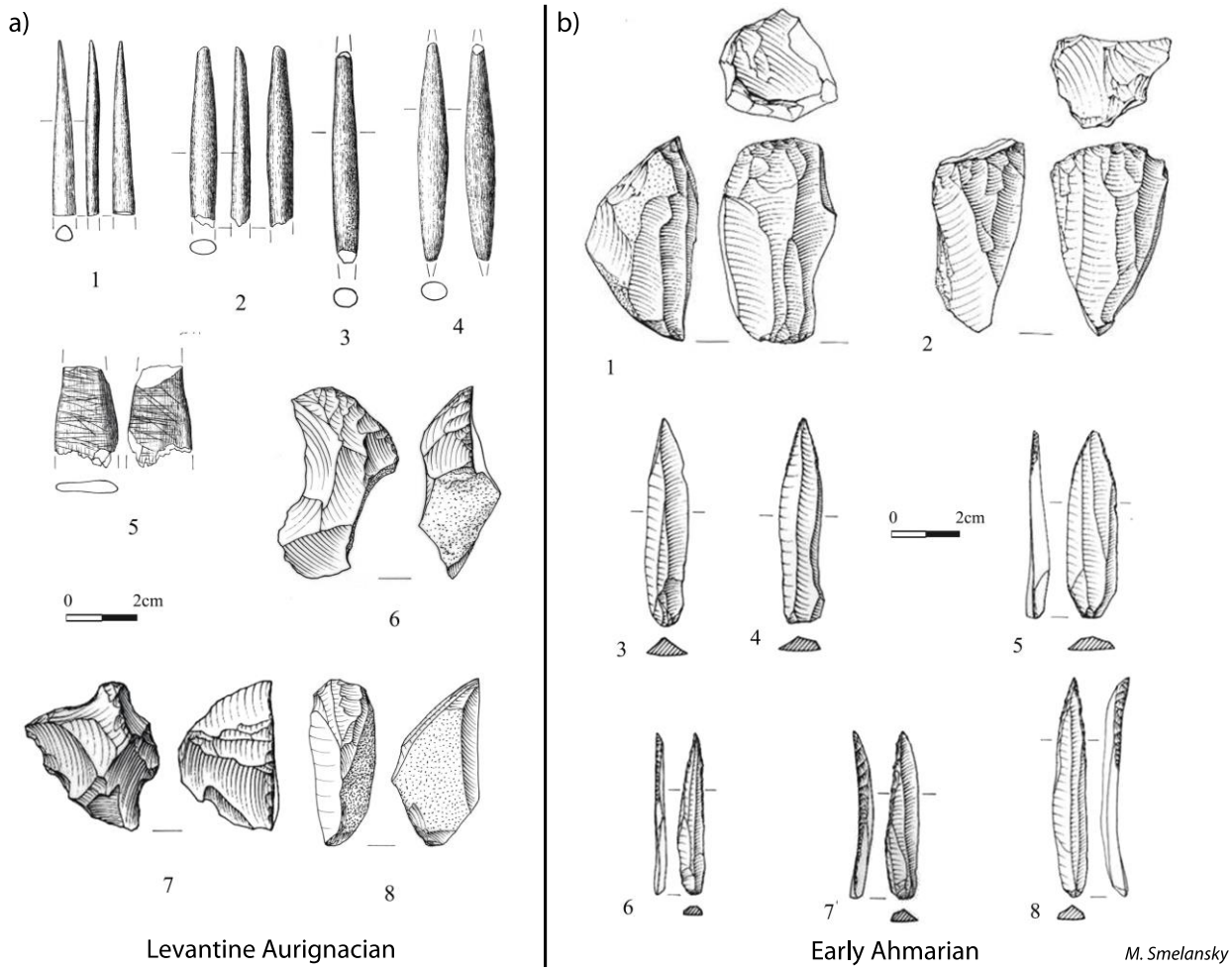

fig. S4. Artifacts from Manot Cave. (A) Levantine Aurignacian artifacts including bone awl (1), antler projectile points (2-4), incised decorated bone (5), carinated and nosed endscrapers (6-8). **(B)** Early Ahmarian artifacts including bidirectional blade core (1), single platform pyramidal blade core (2), and el-Wad points (3-8). Drawn by M. Smelansky.

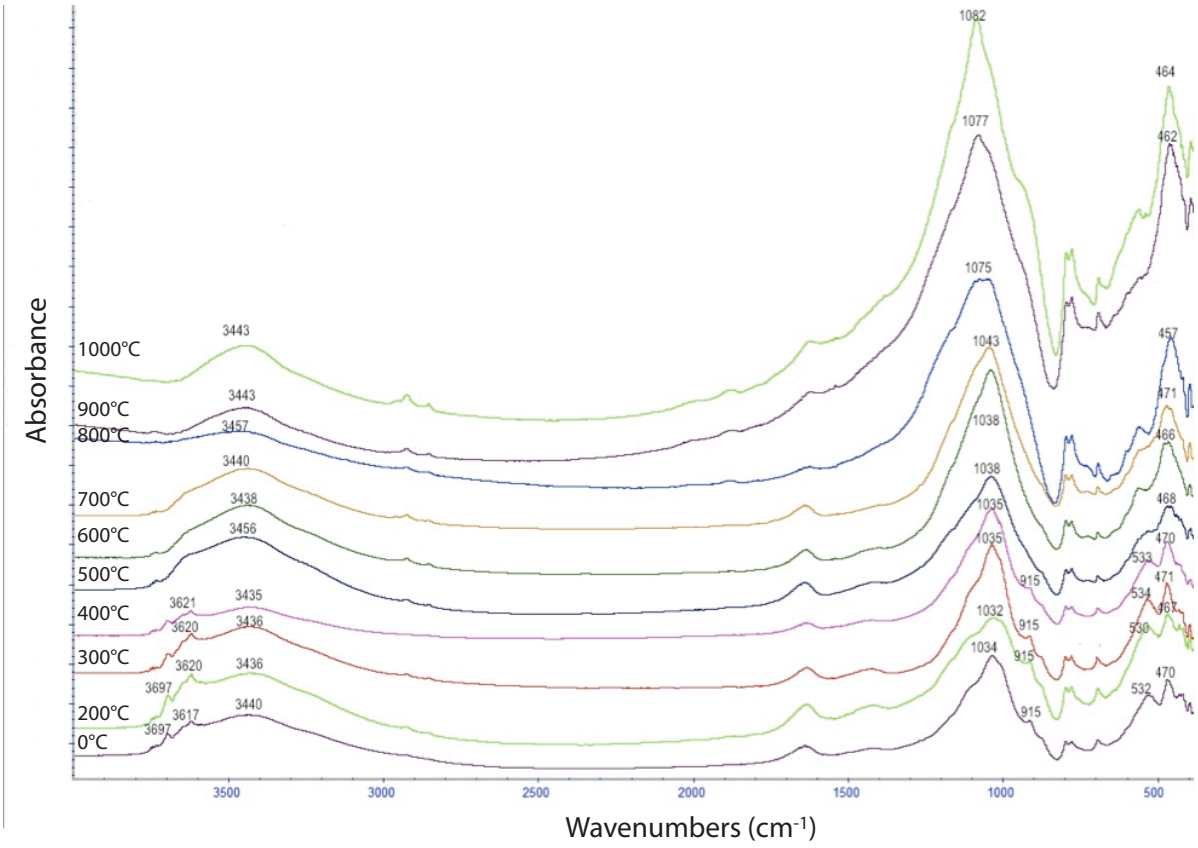

fig. S5. FTIR spectra of sediment exposed to different temperatures in experimental heating study. Above 500°C the kaolinite OH absorption at 3695 cm^{-1} disappears. At 800°C the shoulder at 3620 cm^{-1} disappears and the major Si-O silicate absorption begins to shift from 1035 cm^{-1} to higher wavenumbers (>1070 cm^{-1}). The spectra have been stacked vertically for display and therefore the y-axis represents relative absorption from the baseline of each spectrum and not an absolute value from the axis baseline.

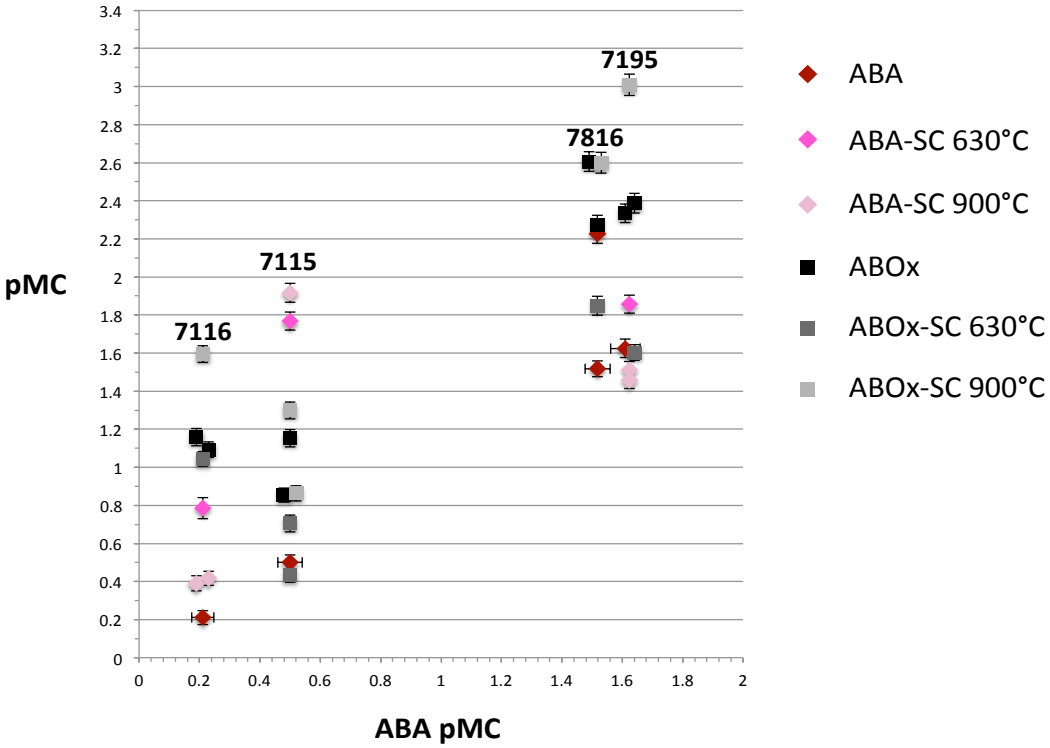

fig. S6. Radiocarbon measurements of Manot charcoal samples prepared by different pretreatments. pMC values of 4 samples prepared by different pretreatments plotted by ABA pMC value for each sample. Overlapping points jittered horizontally for display.

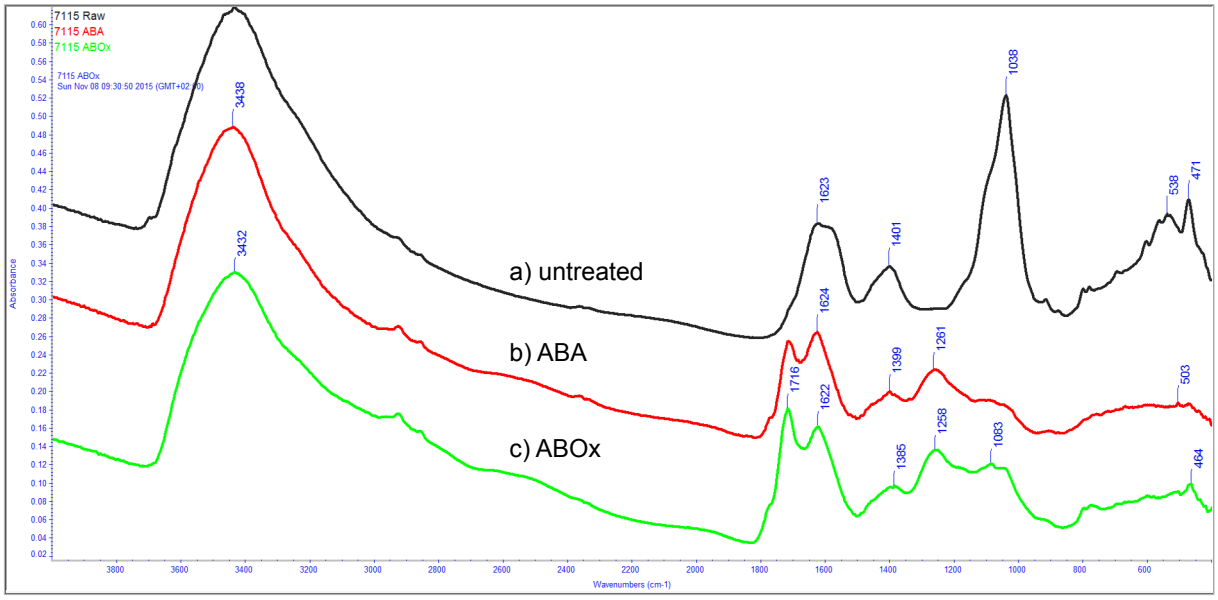

fig. S7. FTIR spectra of charcoal sample before pretreatment, after ABA, and after ABOx. Absorption spectra for sample RTD-7115. **(A)** untreated charcoal, **(B)** ABA treated charcoal and **(C)** ABOx treated charcoal. Absorption peaks at 1716 & 1260 cm^{-1} (COOH) and 1624 & 1400 cm^{-1} (COO^{-}) are related to the charcoal material. Peaks at 1083, 1038, 799-789 cm^{-1} are related to the presence of quartz and clay. These latter peaks are more evident in the ABOx spectrum indicating the possibility of higher contamination. Spectra have been shifted horizontally for comparison and the y-axis represents relative values of absorption from each spectrum's baseline.

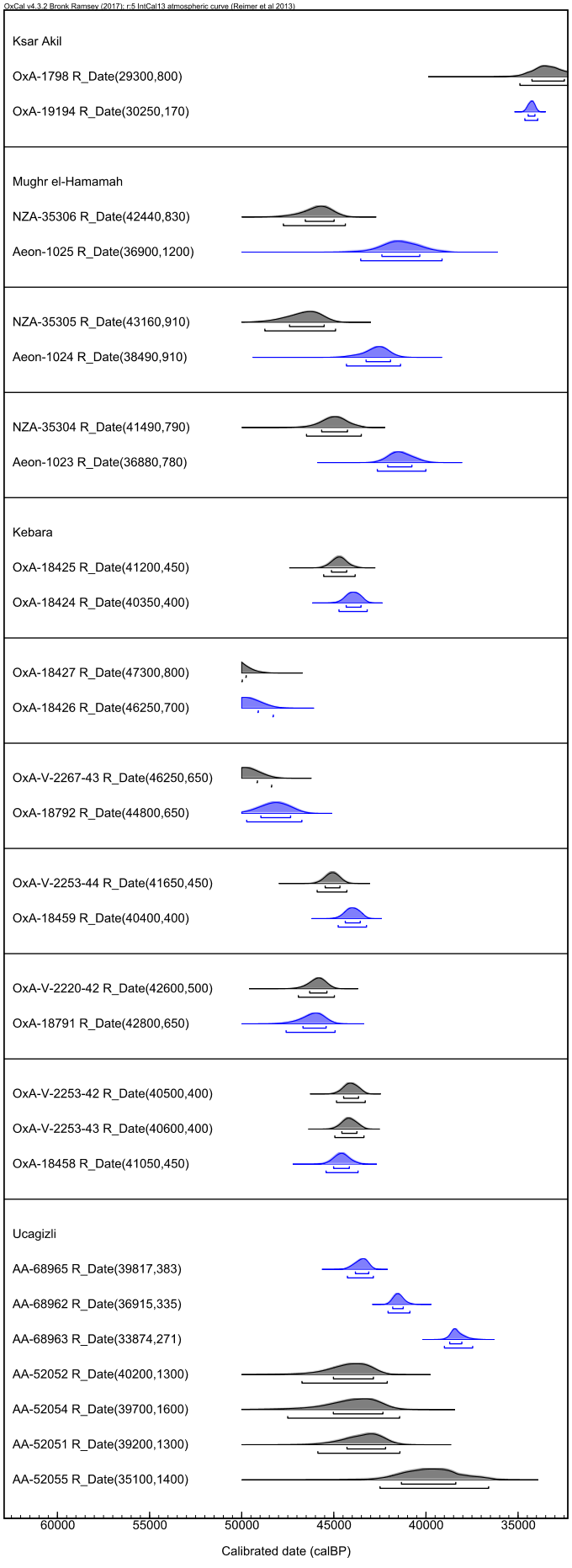
OxCal v4.3.2 Bronk Ramsey (2017); r:5 IntCal13 atmospheric curve (Reimer et al 2013)
Ksar Akil
OxA-1798 R_Date(29300,800)
OxA-19194 R_Date(30250,170)
Mughr el-Hamamah
NZA-35306 R_Date(42440,830)
Aeon-1025 R_Date(36900,1200)
NZA-35305 R_Date(43160,910)
Aeon-1024 R_Date(38490,910)
NZA-35304 R_Date(41490,790)
Aeon-1023 R_Date(36880,780)
Kebara
OxA-18425 R_Date(41200,450)
OxA-18424 R_Date(40350,400)
OxA-18427 R_Date(47300,800)
OxA-18426 R_Date(46250,700)
OxA-V-2267-43 R_Date(46250,650)
OxA-18792 R_Date(44800,650)
OxA-V-2253-44 R_Date(41650,450)
OxA-18459 R_Date(40400,400)
OxA-V-2220-42 R_Date(42600,500)
OxA-18791 R_Date(42800,650)
OxA-V-2253-42 R_Date(40500,400)
OxA-V-2253-43 R_Date(40600,400)
OxA-18458 R_Date(41050,450)
Ucagizli
AA-68965 R_Date(39817,383)
AA-68962 R_Date(36915,335)
AA-68963 R_Date(33874,271)
AA-52052 R_Date(40200,1300)
AA-52054 R_Date(39700,1600)
AA-52051 R_Date(39200,1300)
AA-52055 R_Date(35100,1400)
60000
55000
50000
45000
40000
35000
Calibrated date (calBP)

fig. S8. Comparison of ABA and ABOx charcoal dates from Levantine EUP sites. Dates within each box represent charcoals divided and prepared by ABA (gray) and ABOx (blue), for which both fractions passed quality control. The ABA fractions are either older or statistically indistinguishable from the ABOx fractions. For Üçağızlı individual charcoals were not prepared by both methods, but charcoals from the same Layer I were prepared by ABA (gray) and ABOx (blue).

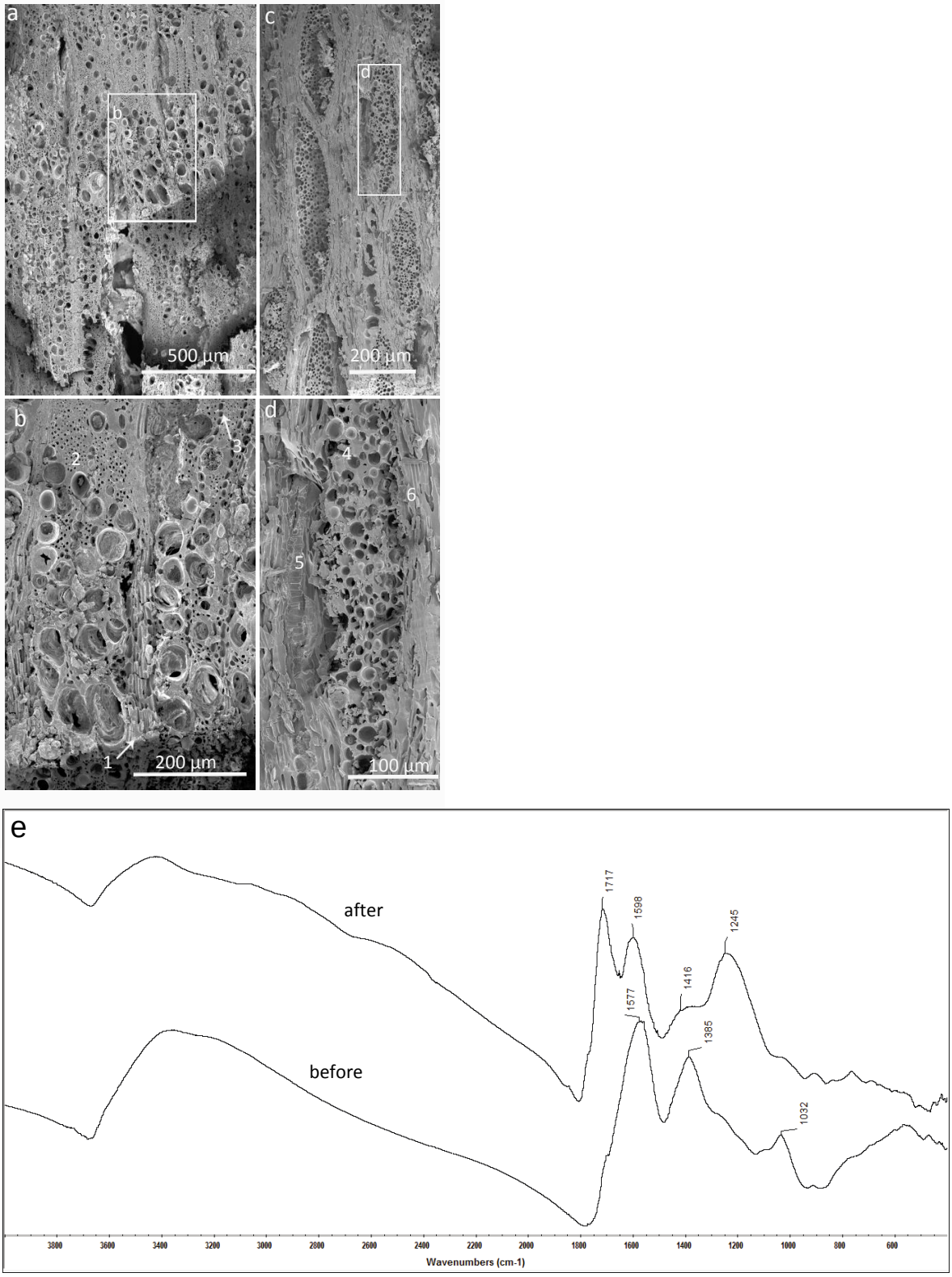

fig. S9. Characterization of *Amygdalus sp*. charcoal by scanning electron microscopy and FTIR. (A) SEM of transverse section showing the distinct pattern of the growth rings. **(B)** Enlarged picture of a portion of wood tissue represented in picture (A). Vessels in radial groups in the early wood and solitary in the late wood. Rays 1 to 5 seriates (features 1 and 3). Parenchyma very sparse, mostly apotracheal and occasionaly paratracheal (feature 2). **(C)** SEM of tangential

section showing the distribution of rays, vessels and fibers. **(D)** Enlarged picture of wood tissue in (C) showing a 5-seriate, 15 cells long ray (feature 4), vessel with spiral thickenings (feature 5), and thick-walled fibers (feature 6). **(E)** FTIR spectra of charcoal sample RTD-7197 before (below) and after (above) ABA pretreatment. The before spectrum shows carboxylate absorptions at 1577 and 1385 cm^{-1}, which are characteristic of fossil charcoal, as well as a silicate absorption at 1032 cm^{-1} indicative of clay. The after spectrum shows the pattern characteristic of ABA treated charcoal (carboxylic acid absorptions at 1717 and 1245 cm^{-1}; carboxylate absorptions at 1598 and 1416 cm^{-1}) and no peaks indicating the presence of clay, suggesting that pretreatment effectively removed this contaminant.

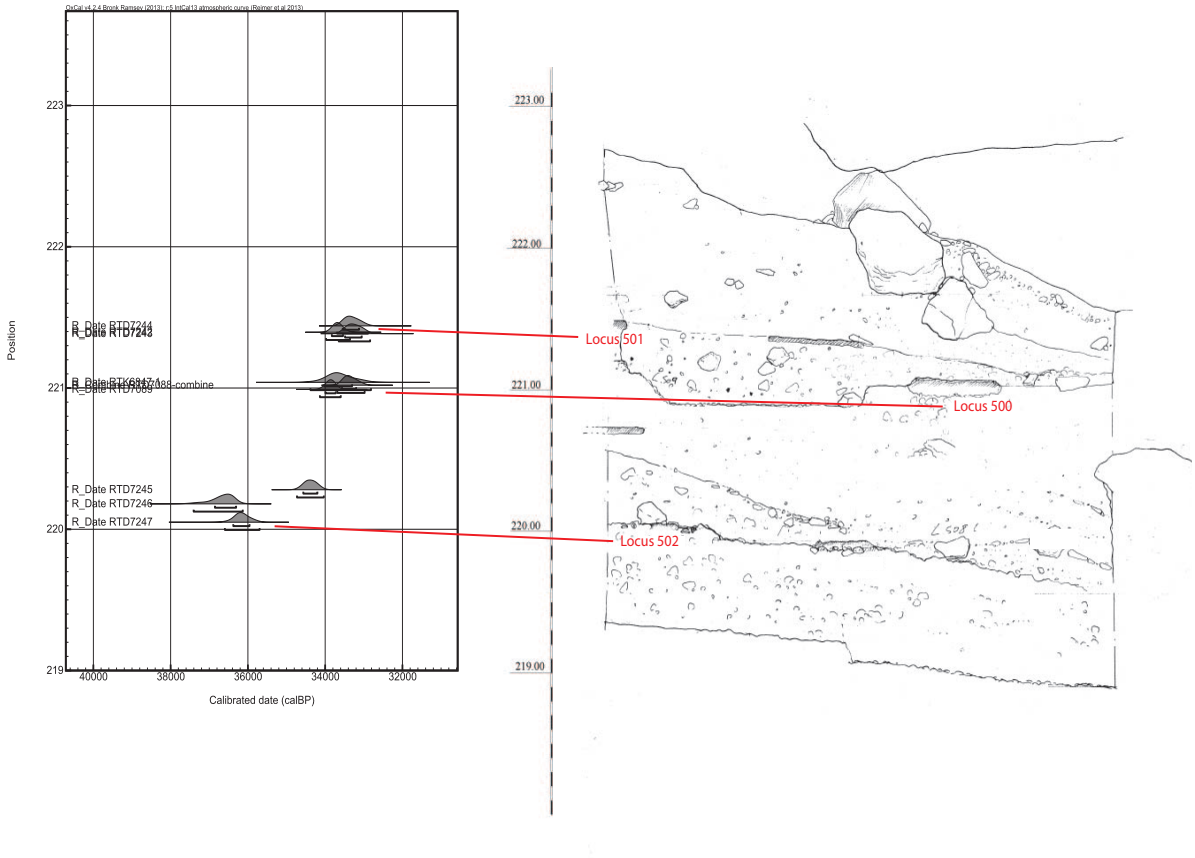

fig. S10. Calibrated radiocarbon dates from area E plotted by absolute elevation. Charcoals came from combustion features (Loci 500, 501, 502) with the exception of RTD-7245, which came from 10 cm above Locus 502 in the Unit 1 colluvium.

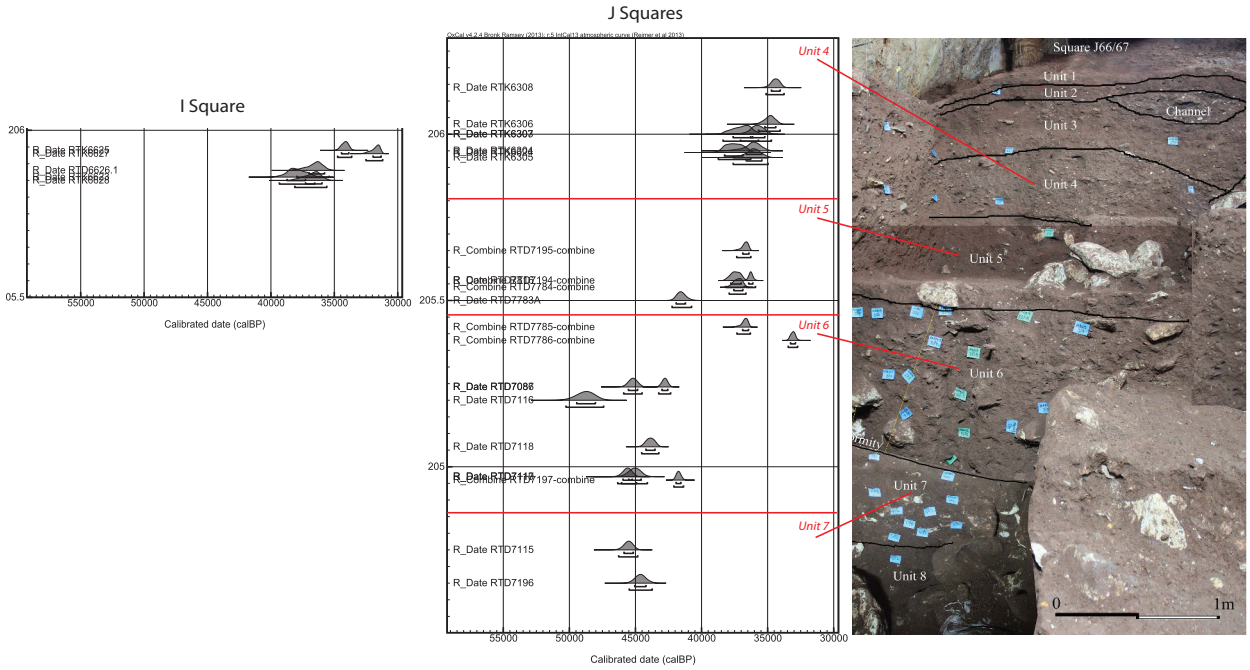

fig. S11. Calibrated radiocarbon dates from area C plotted by absolute elevation. Dates from the J squares (J66, J65, J64) are shown against the stepped section, which contained a well-preserved archaeological sequence. Dates from adjacent square I65 came from a more mixed context next to the cave wall, but are broadly consistent with those from the J squares.

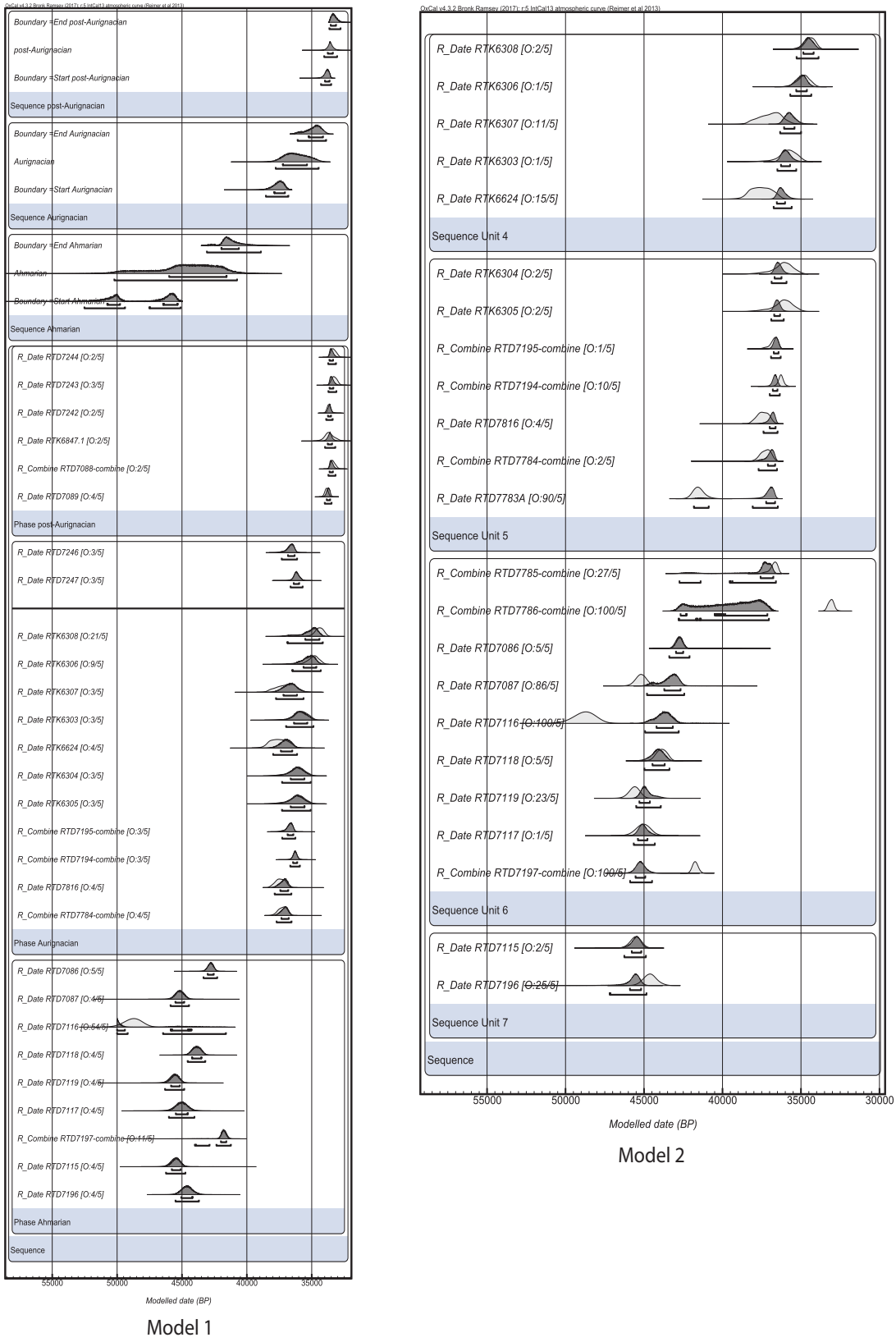

fig. S12. Bayesian models and outlier analysis. Modeled dates are dark gray and unmodeled calibrated dates are light gray. Outlier probabilities are listed after each sample number *[O:*posterior/prior*]*. Model 1 constrained dates to three sequential phases of Ahmarian > Aurignacian > post-Levantine Aurignacian. The modeled spans of phases are shown at the top. Model 2 constrained dates from Area C to four contiguous sequences based on lithostratigraphic layer.

table S1. Lithic assemblage in area E. General breakdown by category of the lithic assemblages from Area E Unit 2 Layers I-IX.

Layer	Debitage		Debris		Tools		Cores		Total
	N	%	N	%	N	%	N	%	
I	293	25.15	839	72.01	30	2.57	3	0.25	1165
II	403	40.3	559	55.9	38	3.8	8	2.2	1000
III	770	49.51	694	44.63	69	1.92	22	0.51	1555
IV	261	50.09	219	42.03	36	6.90	5	0.95	521
V	775	39.2	1061	53.66	117	5.91	24	1.21	1977
VI	508	58.05	252	28.8	78	8.91	37	4.22	875
VII	125	41.39	152	50.33	21	6.95	6	2.12	302
VIII	236	83.68	201	71.27	39	12.82	6	2.12	282
IX	155	41.44	182	48.66	46	12.2	11	2.9	374
Total	**3526**		**4159**		**474**		**122**		**8051**

table S2. Lithic assemblage in area C. General breakdown by category of the lithic assemblages in Area C.

Unit	Debitage		Debris		Tools		Cores		Total
	N	%	N	%	N	%	N	%	
2	114	32.2	223	63.0	15	4.2	2	0.6	354
3	239	50.0	176	36.8	57	11.9	6	1.3	478
4	869	41.9	1104	53.3	77	3.7	22	1.1	2072
5	3187	34.7	5600	61.0	289	3.1	110	1.2	9186
6	1912	44.3	2163	50.1	183	4.2	60	1.4	4318
7	1214	33.5	2228	61.5	115	3.2	67	1.8	3624
8	111	15.5	588	82.1	9	1.3	8	1.1	716
Total	**7646**		**12082**		**745**		**275**		**20748**

table S3. Radiocarbon measurements of Manot charcoal samples prepared by different pretreatments. pMC values for 4 charcoals pretreated by ABA, ABA-SC to 630°C, ABA-SC to 900°C, ABOx, ABOx-SC to 630°C, and ABOx-SC to 900°C.

Sample	Treatment	pMC±1σ	
RTD-7115	ABA	0.5	0.04
	ABA-SC 630	1.768	0.047
	ABA-SC 900	1.916	0.049
	ABOx	1.153	0.046
		0.854	0.038
	ABOx-SC 630	0.705	0.045
		0.433	0.037
	ABOx-SC 900	1.298	0.045
		0.863	0.041
RTD-7116	ABA	0.211	0.037
	ABA-SC 630	0.786	0.056
	ABA-SC 900	0.39	0.039
		0.417	0.038
	ABOx	1.159	0.046
		1.092	0.04
	ABOx-SC 630	1.044	0.038
	ABOx-SC 900	1.594	0.043
RTD-7195	ABA	1.624	0.049
	ABA-SC 630	1.857	0.048
	ABA-SC 900	1.457	0.044
		1.511	0.044
	ABOx	2.387	0.052
		2.334	0.049
	ABOx-SC 630	1.603	0.042
	ABOx-SC 900	3.009	0.056
RTD-7816	ABA	1.518	0.042
		2.227	0.051
	ABOx	2.273	0.052
		2.605	0.052
	ABOx-SC 630	1.849	0.05
	ABOx-SC 900	2.599	0.055

table S4. Comparison of ABA and ABOx charcoal dates from Levantine EUP sites. For Ksâr ʻAkil (*9*), Mughr el-Hamamah (*19*), and Kebara (*8, 15*) individual charcoals were divided and prepared by ABA and ABOx. Each row represents a distinct charcoal with laboratory ID, ^{14}C BP date, and %C for the treatments. Some charcoals had two replicates for a given treatment and therefore a total of three dates. Gray dates were rejected because the %C was <50. The χ^2 column shows the results of the OxCal Combine function, which tests if the radiocarbon dates could be the same age (*100*). The difference column shows the number of years older the ABA fraction could be than the ABOx fraction at 95% confidence. For example from the Kebara Brock & Higham 2009 study, the estimated difference between fractions of charcoal 4/Q15 III Bf was 1900 to -400, meaning the ABA fraction produced a date between 1900 years older to 400 years younger than the ABOx sample. These dates are statistically indistinguishable and could be combined into a single estimate. From Mughr el-Hamamah (MHM), the charcoal MHM 5-325 produced ABA and ABOx dates that failed to combine, with a difference of 7400 to 1760, meaning the ABA fraction was between 7400 to 1760 years older than the ABOx date. No individual charcoals were divided and prepared by both treatments from Üçağızlı, but charcoals from the same layer prepared by both treatments produced overlapping results (*17*).

site	study	charcoal ID	ABA			ABOx			χ^2	difference yrs ABA older
			laboratory ID	14C BP	%C	laboratory ID	14C BP	%C		
Ksar Akil	Douka et al 2013	8ac	OxA-1798	29300 ± 800		OxA-19194	30250 ± 170		combined	690 to -2790
Mughr el-Hamamah	Stutz et al 2015	MHM 5-325	NZA-35306	42440 ± 830		Aeon-1025	36900 ± 1200		failed	7400 to 1760
		MHM 4	NZA-35305	43160 ± 910		Aeon-1024	38490 ± 910		failed	6900 to 1260
		MHM 2	NZA-35304	41490 ± 790		Aeon-1023	36880 ± 780		failed	5660 to 1680
Kebara	Brock & Higham 2009	4/Q15 III Bf	OxA-18425	41200 ± 450	60.5	OxA-18424	40350 ± 400	67.5	combined	1900 to -400
		6/Q14d V	OxA-18427	47300 ± 800	59.4	OxA-18426	46250 ± 700	67	combined	
	Rebollo et al 2011	R19 cV	OxA-V-2267-46	51500 ± 1200	56.6	OxA-18804	44300 ± 1000	21.8	x	
		R19aV_4	OxA-V-2267-45	49600 ± 1000	55.6	OxA-18803	50600 ± 1600	33.1	x	
		R15cV	OxA-V-2267-43	46250 ± 650	62.3	OxA-18792	44800 ± 650	51.7	combined	
		R19aV_2	OxA-V-2253-46	45200 ± 700	53.8	OxA-X-2252-7	36300 ± 650	13.3	x	
		R19aIV_4	OxA-V-2269-35	36110 ± 330	46.7	OxA-X-2264-29	40500 ± 1200	10.6	x	
		R19aIV_2	OxA-V-2253-45	43600 ± 600	55.9	OxA-18402	40300 ± 550	29.5	x	
						OxA-18801	35160 ± 310	27.7	x	
		R17aIV	OxA-V-2253-44	41650 ± 450	69.8	OxA-18459	40400 ± 400	67.7	failed	2220 to -34
		R16cIIIb_1	OxA-V-2220-41	42850 ± 550	59.7	OxA-X-2222-32	41400 ± 1200	49.3	x	
		R17aIIIb,f	OxA-V-2220-42	42600 ± 500	57	OxA-18791	42800 ± 650	64.3	combined	1380 to -1980
		R16cIIIb_2	OxA-V-2253-42	40500 ± 400	58	OxA-18458	41050 ± 450	72.1	combined	680 to -1660
			OxA-V-2253-43	40600 ± 400	60.9				combined	770 to -1580
Üçağızlı Layer I	Kuhn et al 2009					AA-68965	39817 ± 383			
						AA-68962	36915 ± 335			
						AA-68963	33874 ± 271			
			AA-52052	40200 ± 1300						
			AA-52054	39700 ± 1600						
			AA-52051	39200 ± 1300						
			AA-52055	35100 ± 1400						

table S5. Radiocarbon samples and dates for Manot Cave. All samples were *Amygdalus* sp. charcoal, except for those noted as sediment. Sediment and charcoal samples collected together have the same field ID. Samples with RTD before the laboratory code were prepared and measured by AMS at the D-REAMS, Max Planck-Weizmann Center for Integrative Archaeology and Anthropology. Samples with RTK were prepared to graphite in the D-REAMS laboratory and measured at the Arizona AMS Facility, University of Arizona. Percent efficiency (%Eff) is the percent by dry weight that survived pretreatment. Percent carbon (%C) was measured upon combustion. The treatments are acid-base-acid (ABA), water-base-acid (WBA), or acid (A, for sediments only). Samples graphitized on the ultraclean vacuum are noted as "uc line" after treatment. Gray text indicates replicate samples that were either included as a combined date or rejected because of preservation parameters. Calibrations use IntCal13 (*60*) and OxCal v4.2 (*59*).

Laboratory ID	Field ID	Square	Elevation	Unit-Layer	^{14}C BP	calBP (68.2%)	δ^{13}C	%Eff	%C	treatment
AREA E										
Combustion feature locus 501 (221.56-221.46)										
RTD-7244	MAN13-358	SY92	221.46-221.42	2-I	29090 ± 150	33550-33120	-23.1	36	59	ABA
RTD-7243	MAN13-357	SY92c	221.41-221.36	2-I	29030 ± 150	33490-33050	-24.4	32	46	ABA
RTD-7242	MAN13-356	SY92	221.41-221.38	2-I	29460 ± 150	33830-33540		12	43	ABA
Combustion feature locus 500 (221.04-220.95)										
RTK-6847.1	MANC-2	A92		2-I	29500 ± 380	34030-33300		23	76	ABA
RTD-7088 combine	MAN13-340	B92	221.02	2-I		33570-33200	-23.1			
RTD-7088A					29230 ± 200	33710-33240		48	74	WBA
RTD-7088B					29060 ± 150	33520-33090		33	65	ABA
RTD-7089	MAN13-341	A92	220.99	2-I	29720 ± 150	33990-33730	-23.3	40	78	WBA
Unit 1 colluvium										
RTD-7245	MAN13-359	SY89d	220.37-220.19	1	30390 ± 170	34570-34200	-26.3	29	43	ABA
Combustion feature locus 502 (220.07-220.03)										
RTD-7246	MAN13-360	SY89	220.18	2-IV	32690 ± 200	36860-36310	-25.1	30	64	ABA
RTD-7247	MAN13-363	SY89	220.08-220.02	2-IV	32270 ± 190	36380-35960	-25	36	68	ABA
AREA C										
J squares sequence										
RTK-6308	Manot10-13	J65a	206.14	4	30400 ± 400	34720-34050	-24.8	24	68	ABA

RTK-6306	Manot10-10	J65b	206.03	4	30900 ± 420	35210-34380	-25.2	60	64	ABA
RTK-6307	Manot10-11	J65b	206.00	4	32700 ± 530	37610-36140	-26.6	61	66	ABA
RTK-6303	Manot10-7	J65b	206.00	4	31900 ± 500	36280-35220	-25.1	56	61	ABA
RTK-6624	B3533	J65d	205.95-205.94	4	33300 ± 500	38260-36860	-24.9	10	61	ABA
RTK-6304	Manot10-8	J65b	205.95	5	32100 ± 500	36620-35440	-24.1	59	65	ABA
RTK-6305	Manot10-9	J65b	205.93	5	32100 ± 500	36620-35440	-24.5	43	69	ABA
RTD-7195 combine (failed)	MAN13-355	J66cd	205.7-205.6	5		36880-36410	-25.1	37		
RTD-7195.1					33130 ± 210	37710-36840				ABA
RTD-7195.2					32380 ± 200	36490-36050				ABA
RTD-7194 combine	MAN13-353	J66cd	205.6-205.52	5		36430-36120	-25.9	44		
RTD-7194.1					32240 ± 190	36350-35930			85	ABA
RTD-7194.2					32540 ± 200	36680-36200				ABA
RTD-7816	C119/12	J65cd	205.56	5	33210 ± 160	37780-37000		37	68	ABA
RTD-7784 combine (failed)	C137/12	J65a	205.54	5		37560-36880		32		
RTD-7784.1					33740 ± 290	38600-37810			71	ABA-uc line
RTD-7784.2					32920 ± 150	37190-36560			73	ABA
RTD-7783	C129/12	J65cd	205.5	5						
RTD-7783A					36990 ± 430	41920-41220		5	75	ABA-uc line
RTD-7783B					31260 ± 140			17	37	ABA
RTD-7785 combine	C174/12	J65c	205.42	6		36890-36450		26		
RTD-7785.1					32410 ± 260	36610-36010			90	ABA-uc line
RTD-7785.2					32900 ± 150	37140-36530			62	ABA
RTD-7786 combine	C188/12	J65b	205.38	6		33270-32900		41		
RTD-7786.1					28940 ± 180	33420-32910			82	ABA-uc line

RTD-7786.2					28850 ± 100	33250-32860			67	ABA
RTD-7086	MAN13-331B.1	J66/65	205.31-205.16	6	38880 ± 310	43000-42550		37	71	WBA
RTD-7087	MAN13-331B.2	J66/65	205.31-205.16	6	41790 ± 380	45530-44840	-23.2	62	45	WBA
RTD-7116	MAN13-347	J65ab	205.25-205.14	6	48700 ± 700	49440-48030	-28.3	26	70	ABA
RTD-7128B	MAN13-347 sediment	J65ab	205.25-205.14	6	28560 ± 150	32920-32310		64	0.6	A
RTD-7118	MAN13-315	J66/65	205.06	6	40280 ± 320	44210-43520	-25.2	17	54	ABA
RTD-7119	MAN13-350	J65	205.04-204.90	6	42310 ± 380	45940-45250	-23.8	21	69	ABA
RTD-7130B	MAN13-350 sediment	J65	205.04-204.90	6	30860 ± 180	35030-34670		53	0.6	A
RTD-7117	MAN13-349	J65	205.03-204.91	6	41610 ± 540	45510-44570	-24.8	37	67	ABA
RTD-7129B	MAN13-349 sediment	J65	205.03-204.91	6	31270 ± 190	35360-34910		67	0.5	A
RTD-7197 combine	MAN13-351	J64ab	205.02-204.90	6		41930-41560	-23.4	19		
RTD7197.1					37330 ± 300	42040-41580			86	ABA
RTD7197.2					37120 ± 300	41910-41430				ABA
RTD-7115	MAN13-346	J65	204.80-204.70	7	42210 ± 390	45870-45160	-25.6	27	>40	ABA
RTD-7127B	MAN13-346 sediment	J65	204.80-204.70	7	25080 ± 110	29280-28940		62	0.8	A
RTD-7196	MAN13-348	J65cd	204.70-204.60	7	41100 ± 450	45050-44200	-24.3	18	81	ABA
I square sequence										
RTK-6849	MAN11-108 sediment	I65	206.29	-	21550 ± 160	25970-25710				A
RTK-6848	MAN11-107 sediment	I65	206.00	-	24430 ± 210	28700-28240				A
RTK-6625	B3534	I65	205.96-205.91	-	30100 ± 340	34430-33860	-24.3	38	65	ABA
RTK-6627	B3525	I65	205.95-205.90	-	27900 ± 260	31950-31310	-24.7	32	63	ABA
RTK-6626.1	B3535	I65	205.90-205.86	-	32400 ± 460	36990-35770	-25.9	42	59	ABA
RTK-6623	B3541	I65	205.87-205.85	-	33700 ± 530	38730-37280	-25.0	65	71	ABA

RTK-6628	B3538	I65	205.85	-	32600 ± 460	37270-35970	-24.6	31	65	ABA
M square between flowstones										
RTK-6704	C 047/12	M65a	206.23		23600 ± 200	27870-27570	-24.9		57	ABA
RTK-6705	C 062/12	M65a	206.14		23200 ± 190	27630-27330	-23.7		78	ABA
RTK-6706	C 067/12	M65a	206.10		25900 ± 280	31170-30840	-23.0		78	ABA
RTK-6708	C 077/12	M65a	206.05		24000 ± 210	28350-27890	-23.5		55	ABA

table S6. Excavation contexts with archeological classifications and date ranges. For Area C, the table only includes J-squares used to construct the cultural chronology. Dates from I and M squares (included in Table S5) were used to understand site formation processes and check U-Th dates.

Area	Unit	Layer	Cultural phase	Context	Date range cal BP 68.2% (*sample number*)
E	1		sterile	colluvium	34,600-34,200 (*1*)
	2	I-III	Post-Levantine Aurignacian	*In situ* occupational surfaces	34,000-33,100 (*6*)
		IV-IX	Levantine Aurignacian	*In situ* occupational surfaces	36,900-36,000 (*2*)
C	4		Levantine Aurignacian	Secondary talus deposit	38,300-34,100 (*5*)
	5		Levantine Aurignacian/ Ahmarian	Secondary talus deposit	42,000-35,400 (*7*)
	6		Levantine Aurignacian/ Ahmarian	Secondary talus deposit	49,400-33,000 (*9*)
	7		Ahmarian	Secondary talus deposit	45,900-44,200 (*2*)
	8		Ahmarian, some IUP and MP	Secondary talus deposit	

table S7. Outputs of Bayesian model 1 based on cultural phases. Cultural span model (Model 1) constrained dates to three sequential phases of Ahmarian > Aurignacian > post-Levantine Aurignacian. Only 1/28 dates is identified as an outlier.

Phase	**Contexts**	**Sample**	**Modeled date (68.2%)**		**Outlier likelihood %**
			from	to	
Post-Levantine Aurignacian 33,766-33,365	Area E Unit 2 Layer I	RTD-7244	33634	33350	2
		RTD-7243	33625	33331	3
		RTD-7242	33750	33509	2
		RTK-6847.1	33768	33426	2
		RTD-7088	33627	33365	2
		RTD-7089	33842	33577	4
Aurignacian 37,222-35,361	Area E Unit 2 Layer IV	RTD-7246	36832	36314	3
		RTD-7247	36389	35963	3
	Area C Unit 4	RTK-6308	35497	34398	21
		RTK-6306	35633	34639	9
		RTK-6307	37182	36135	3
		RTK-6303	36370	35333	3
		RTK-6624	37382	36496	4
	Area C Unit 5 (above z=205.50)	RTK-6304	36623	35559	3
		RTK-6305	36624	35551	3
		RTD-7195	36862	36411	3
		RTD-7194	36440	36116	3
		RTD-7816	37424	36806	4
		RTD-7784	37336	36770	4
Ahmarian 45,988-41,559	Area C Unit 6 (below z= 205.35)	RTD-7086	43019	42548	5
		RTD-7087	45508	44822	4
		RTD-7116	50005	44262	54
		RTD-7118	44224	43500	4
		RTD-7119	45843	45161	4
		RTD-7117	45476	44550	4
		RTD-7197	42000	41579	11
	Area C Unit 7	RTD-7115	45786	45099	4
		RTD-7196	45058	44190	4

table S8. Cultural phase estimates for eight runs of model 1. Outputs of eight runs of Model 1 showing the posterior outlier likelihood for sample RTD-7116 and cultural phases ranges estimated by the OxCal Date function. The model does not produce consistent results for the start of the Ahmarian and outlier probability of RTD-7116.

Run	RTD-7116 outlier %	Ahmarian	Aurignacian	Post-Levantine Aurignacian
1	54	45,988 - 41,559	37,222 - 35,361	33,766 - 33,365
2	7	49,318 - 41,937	37,201 - 35,273	33,756 - 33,375
3	60	45,793 - 41,729	37,233 - 35,340	33,751 - 33,381
4	29	47,753 - 41,443	37,212 - 35,229	33,806 - 33,307
5	83	45,551 - 42,048	37,229 - 35,497	33,761 - 33,378
6	55	45,873 - 41,624	37,220 - 35,363	33,767 - 33,366
7	5	49,356 - 41,903	37,191 - 35,300	33,755 - 33,378
8	14	48,391 - 41,795	37,173 - 35,269	33,758 - 33,372

table S9. Outputs of Bayesian model 2 based on lithostratigraphic units. Model 2 constrained dates from Area C to four contiguous sequences based on lithostratigraphic unit. 5/23 dates were identified as outliers.

Phase	**Sample**	**Modeled date (68.2%)**		**Outlier %**
		From	**to**	
Unit 4	RTK-6308	34850	34192	2
	RTK-6306	35302	34622	1
	RTK-6307	36078	35409	11
	RTK-6303	36275	35694	1
	RTK-6624	36539	36013	15
Unit 5	RTK-6304	36682	36239	2
	RTK-6305	36706	36331	2
	RTD-7195	36733	36428	1
	RTD-7194	36797	36496	10
	RTD-7816	36992	36616	4
	RTD-7784	37111	36644	2
	RTD-7783A	37219	36648	90
Unit 6	RTD-7785	37575	36760	27
	RTD-7786	42671	37140	100
	RTD-7086	42965	42501	5
	RTD-7087	43710	42670	86
	RTD-7116	44203	43162	100
	RTD-7118	44463	43680	5
	RTD-7119	45296	44625	23
	RTD-7117	45390	44780	1
	RTD-7197	45541	44920	100
Unit 7	RTD-7115	45781	45172	2
	RTD-7196	45897	45186	25